26 Suzuki M, Shinkai M, Honda H, Kobayashi T. Anticancer effect and immune induction by hyperthermia of malignant melanoma using magnetite cationic liposomes. *Melanoma Res* 2003; 13: 129–35.
27 Kano E, Miyakoshi J, Sugahara T. Difference in sensitivities to hyperthermia and ionizing radiation of various mammalian cell stress *in vitro*. In: Streffer C, Van Beuninen D, Dietzel F *et al.*, eds. *Cancer Therapy by Hyperthermia and Radiation*. Baltimore-Munich: Urban and Schwarzenberg, 1978: 188–90.
28 Kano E, Miyakoshi J, Furukawa M *et al.* Effects of hyperthermia at 50 degrees C on V-79 cells *in vitro*. *J Radiat Res (Tokyo)* 1982; 23: 218–27.
29 Ito A, Nakahara Y, Tanaka K, Kuga Y, Honda H, Kobayashi T. Time course of biodistribution and heat generation of magnetite cationic liposomes in mouse model. *Jpn J Hyperthermic Oncol* 2003; 19: 151–9.
30 Ito Y, Jimbow K, Ito S. Depigmentation of black guinea pig skin by topical application of cysteaminylphenol, cysteinylphenol, and related compounds. *J Invest Dermatol* 1987; 88: 77–82.
31 Ito Y, Jimbow K. Selective cytotoxicity of 4-*S*-cysteaminylphenol on follicular melanocytes of the black mouse: rational basis for its application to melanoma chemotherapy. *Cancer Res* 1987; 47: 3278–84.
32 Inoue S, Ito S, Wakamatsu K, Jimbow K, Fujita K. Mechanism of growth inhibition of melanoma cells by 4-*S*-cysteaminylphenol and its analogues. *Biochem Pharmacol* 1990; 39: 1077–83.

doi: 10.1111/j.1349-7006.2006.00382.x

Human Molecular Genetics, 2007, Vol. 16, No. 1 **50–60**
doi:10.1093/hmg/ddl439
Advance Access published on November 20, 2006

Pael receptor induces death of dopaminergic neurons in the substantia nigra via endoplasmic reticulum stress and dopamine toxicity, which is enhanced under condition of parkin inactivation

Yasuko Kitao[1,*,†], Yuzuru Imai[2,†], Kentaro Ozawa[1], Ayane Kataoka[2], Toshio Ikeda[3], Mariko Soda[2], Kazuhiko Nakimawa[4], Hiroshi Kiyama[4], David M. Stern[7], Osamu Hori[1], Kazumasa Wakamatsu[6], Shosuke Ito[6], Shigeyoshi Itohara[3], Ryosuke Takahashi[2,5,†] and Satoshi Ogawa[1,†]

[1]Department of Neuroanatomy, Kanazawa University Medical School, 13-1, Takara-machi, Kanazawa City, 920-8640 Ishikawa, Japan, [2]Laboratory for Motor System Neurodegeneration and [3]Laboratory for Behavioral Genetics and RIKEN Brain Science Institute (BSI), Saitama 351-0198, Japan, [4]Department of Anatomy and Neurobiology, Osaka City University, Graduate School of Medicine, Osaka, Japan, [5]Department of Neurology, Kyoto University Medical School, Kyoto, Japan, [6]Department of Chemistry, Fujita Health University School of Health Sciences, Aichi 470-1192, Japan and [7]Dean's Office, College of Medicine, University of Cincinnati, Cincinnati, OH 45267, USA

Received August 2, 2006; Revised October 19, 2006; Accepted November 13, 2006

Selective loss of dopaminergic neurons is the final common pathway in Parkinson's disease. Expression of Parkin associated endothelin-receptor like receptor (Pael-R) in mouse brain was achieved by injecting adenoviral vectors carrying a modified neuron-specific promoter and Cre recombinase into the striatum. Upregulation of Pael-R in the substantia nigra pars compacta of mice by retrograde infection induced endoplasmic reticulum (ER) stress leads to death of dopaminergic neurons. The role of ER stress in dopaminergic neuronal vulnerability was highlighted by their decreased survival in mice deficient in the ubiquitin-protein ligase Parkin and the ER chaperone ORP150 (150 kDa oxygen-regulated protein). Dopamine-related toxicity was also a key factor, as a dopamine synthesis inhibitor blocked neuronal death in parkin null mice. These data suggest a model in which ER- and dopamine-related stress are major contributors to decreased viability of dopaminergic neurons in a setting relevant to Parkinson's disease.

INTRODUCTION

Though Parkinson's disease (PD) is a major contributor to disability and death in the aging population, the molecular basis of selective dopaminergic neuronal toxicity is still under investigation. Progression of the clinical syndrome associated with PD, which includes a well-characterized movement disorder, correlates closely with inexorable loss of neurons in the substantia nigra pars compacta (SNpc) (1).

Mutations in the *Parkin* gene (2) have been identified in the autosomal recessive form of PD (AR-JP), a major cause of juvenile PD. Parkin is a 465 amino acid polypeptide with properties of an ubiquitin-protein ligase (E3) whose N-terminus displays homology to ubiquitin and C-terminus is comprised of two RING fingers flanking a cysteine-rich domain, termed in between RING fingers (IBR) (3–5). Consistent with this view, AR-JP-linked parkin mutants are defective in E3 activity (6–8).

A putative G protein-coupled transmembrane polypeptide, Pael Receptor [Parkin-associated endothelin-receptor like receptor (Pael-R)], has been identified as a Parkin substrate (9). Expression of Pael-R in cultured cells results in accumulation

*To whom correspondence should be addressed. Tel: +81 762652162; Fax: +81 762344222; Email: kitao@nanat.m.kanazawa-u.ac.jp
†These authors equally contributed to this work.

of unfolded, insoluble and ubiquinated Pael-R in the ER, eventuating in ER stress, as indicated by upregulation of chaperones, such as GRP78/BiP, and subsequent neuronal death (10). Overexpression of Parkin in this *in vitro* model resulted in removal/degradation of accumulated Pael-R and increased cell viability. The relevance of ER stress in the central nervous system to pathologic situations and normal neuronal development is suggested by induction of the unfolded protein response (UPR) in cell stress associated with cerebral ischemia (11,12) and exposure to excitatory amino acids (13), as well as during rapid neuronal growth in the neonatal period (14). Salient features of the UPR include upregulation of ER chaperones, suppression of general translation, and activation of the upiquitin-proteasome pathway.

A key facet of the pathology of PD is limitation of cell loss to dopaminergic neurons, especially in the SNpc. In this context, studies of Pael-R might be especially relevant. Pan-neuronal expression of Pael-R in *Drosophila* brain caused selective, age-dependent degeneration of dopaminergic neurons (10). Thus, increased levels of Pael-R render dopaminergic neurons vulnerable to cell death. In the current study, we have found that increased expression of Pael-R in mice in the SNpc results in neuronal death which is accentuated by suppression of Parkin (in $Parkin^{-/-}$ mice) or an ER chaperone (in $Orp150^{+/-}$ mice). In contrast, a dopamine (DA) synthesis inhibitor had neuroprotective properties in this system. Thus, we propose a unified model for cytotoxicity in PD through which a combination of ER stress and dopamine toxicity, potentially acting in concert with mitochondrial dysfunction, result in an ascending cycle of cellular perturbation and, ultimately, death of dopaminergic neurons.

RESULTS

Retrograde and neuron-specific gene expression by adenoviral vectors in the SNpc

It was essential to develop a system with cell-specific protein expression which could be targeted to the SNpc. For this purpose, we established two adenoviral vectors in which nuclear Cre-recombinase was driven by cell-specific promoters; for neuronal expression, we employed AxS2NPNCre (abbreviated as S2NPNCre) with a modified SCG10 promoter (superior cervical ganglia neural-specific 10 protein), and for glial-specific expression, we utilized AxGFAPNCre (abbreviated as GFAPNCre) with the glial fibrillary acidic protein promoter (Fig. 1A). When either of these adenoviral vectors was co-infected with AxCALNLEGFP (abbreviated as LoxEGFP), specific expression of EGFP occurred in neurons (with S2NPNCre) or astrocytes (with GFAPNCre) in a cell culture system (not shown). *In vivo*expression studies were performed in mice by co-infecting either S2NPNCre with LoxEGFP, or GFAPNCre with LoxEGFP. Spatial limitation of gene expression was achieved by injecting viral vectors into the striatum (Fig. 1B), resulting in expression of EGFP protein in the ipsilateral SNpc (Fig. 1C, top panel). When S2NPNCre was injected with LoxEGFP, expression of EGFP (marking neurons) and tyrosine hydroxylase [TH; marking dopaminergic neurons in the SNpc (15)] overlapped (Fig. 1C; middle set of panels); quantitation of this overlap by image analysis, based on studying multiple fields, confirmed extensive coexpression of EGFP with TH (Fig. 1D). In contrast, there was no overlap of EGFP, following injection of S2NPNCre with LoxEGFP, when immunostaining was performed to visualize GFAP (Fig. 1C, lowest set of panels and Fig. 1D). These data indicate that co-infection of the striatum with recombinant adenoviral vectors encoding cell-specific Cre recombinase and EGFP (or other transgenes) flanked by lox P sites, leads to retrograde transport of adenovirus in the nigrostriatal system resulting in gene expression in the SNpc.

Expression of Pael-R in the SNpc activates the unfolded protein response

Using this adenoviral system, we sought to express Pael-R in the SNpc. For this purpose, an adenoviral vector was made with expression of Pael-R under control of the SCG10 promoter regulated by the LoxP system (16), AxCALNLPael-R (abbreviated as LoxPael-R; Fig. 2A). Co-injection of the two adenoviral vectors, S2NPNCre and LoxPael-R, into the striatum increased expression of Pael-R in the SNpc (Fig. 2B, referred to as ipsilateral side). Enhanced expression of Pael-R required both vectors to be co-injected, and was specific for neurons.

Based on previous *in vitro* findings, increased expression of Pael-R in dopaminergic neurons might result in ER stress and diminished cell viability (9). Control experiments were performed by co-injecting three adenoviral vectors, S2NPNCre, LoxEGFP and LoxLacZ, into the striatum on one side of the brain, referred to as contralateral (Fig. 2C, upper panels). Expression of an ER chaperone, ORP150 (oxygen-regulated protein 150), known to increase with ER stress (11), was assessed in neurons expressing EGFP (Fig. 2C, upper panels). ORP150 levels, assessed by Western blotting, were unchanged in the SNpc following injection of this combination of adenoviral vectors (Fig. 2D, left portion and Fig. 2E, middle panel, open bars). Faint ORP150 staining was demonstrated in multiple cells and a much stronger signal for EGFP was observed (Fig. 2C, upper panels). ORP150 has a putative ATPase domain and protein binding site, suggesting that it may have a chaperone-like role in maintaining ER function under stress [(17), and see below]. In this context, we have demonstrated that overexpression of ORP150 rescues neurons from cell death mediated by ischemia (11,12) and excitatory amino acids (13). When S2NPNCre, LoxEGFP and LoxPael-R were injected into the striatum on the ipsilateral side of the brain (the vectors with LoxLacZ in place of LoxPael-R were injected on the contralateral side), a prominent increase in Pael-R in the SNpc (Fig, 2D, right portion) was accompanied by increased expression of ORP150 (Fig. 2C, lower panels) in Pael-R expressing neuron (labeled with EGFP). Western blotting indicated that increased expression of ER chaperones, GRP78 and ORP150, reached a maximum by 7–12 days after infection (Fig, 2D, right portion). In contrast, there was no increase in these chaperones on the contralateral side (i.e. the side where the LoxPael-R adenoviral vector was replace by a LoxLacZ vector; Fig. 2D and E). Levels of a cytoplasmic chaperone, the 70 kDa heat shock protein, remained unchanged on both sides of the brain (Fig. 2D). These data indicate that co-infection of

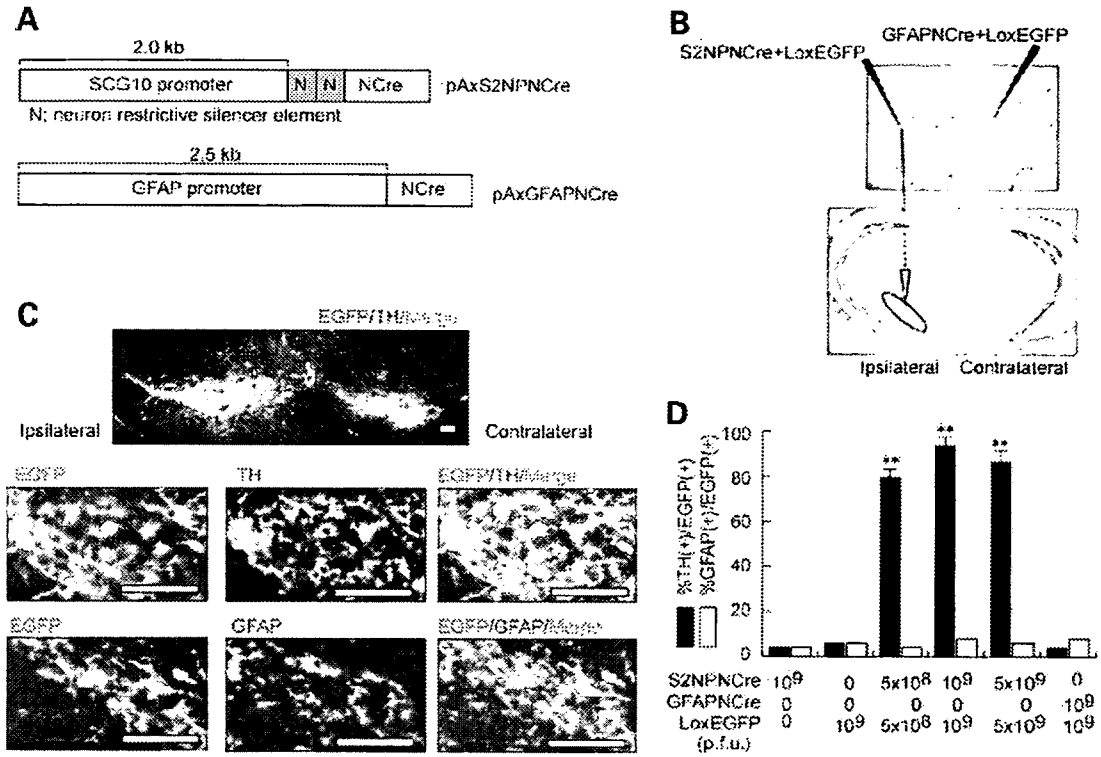

Figure 1. Neuron-specific expression of a transgene in the SNpc after adenoviral infection of the striatum. Two adenoviral vectors were constructed to drive cell type-specific expression of Cre recombinase in neurons (AxS2NPNCre also termed S2NPNCre) and astrocytes (AxGFAPNCre also termed GFAPNCre) (**A**). S2NPNCre was injected unilaterally along with LoxEGFP into the striatum (10^9 p.f.u., in each case) as shown (**B**, upper panel). 7 days after injection, brain slices corresponding to the striatum (B, upper panel) or SNpc (B, lower panel) were analyzed by Nissl staining. On the contralateral side, GFAPNCre was injected along with LoxEGFP (10^9 p.f.u., in each case). SNpc sections were analyzed by fluorescence microscopy using antibodies to TH or GFAP (**C**). Merged images are shown on the top and the far right (marker bar corresponds to 200 μm; note that magnification is greater in the lower panels compared with the top panel), and are representative of six repeat experiments, obtained at −3.1 mM from the Bregma. (**D**) Combinations of adenoviral vectors at the indicated concentrations were injected into the striatum of wild-type mice, and, 7 days later, animals were sacrificed and sections of SNpc were analyzed at five different levels (−3.16, −3.28, −3.40, −3.52 and −3.64 mM from the Bregma). Sections were subjected to image analysis in order to determine the area of TH-positivity [TH(+)] as a percentage of the area of EGFP-positivity [%TH(+)/EGFP(+)]. The mean ± SD is shown ($n = 6$), and ** denotes $P < 0.01$, compared to S2NPNCre infection alone.

LoxPael-R and S2NPNCre in the striatum caused expression of Pael-R in SNpc neurons, and triggered the ER stress.

Expression of Pael-R in SNpc of parkin$^{-/-}$ mice resulted in neuronal death

Parkin null mice (*Parkin*$^{-/-}$) were generated by replacing the proximal exon 3 with a neo cassette (PGK-neo) and two lox P sites (Supplementary Material, Fig. S1A). Southern blotting revealed homologous recombination of the mutant allele (Supplementary Material, Fig. S1B). Reverse transcriptase–polymerase chain reaction (RT–PCR) to detect Parkin transcripts confirmed the absence of normal transcripts in homozygous mutant mice (Supplementary Material, Fig. S1C). Sequencing of RT–PCR products confirmed complete deletion of exon 3 and a frame-shift downstream of exon 2 in mutant mice (Supplementary Material, Fig. S1D). Consistent with these data, western blotting with anti-Parkin antibodies showed the absence of Parkin antigen in brain samples (Supplementary Material, Fig. S1E). Parkin homozygous mutant mice were born at the expected mendelian ratio, showed no overt abnormalities (except a slight decrease in body weight) and had normal lifespans (18,19). Moreover, *Parkin*$^{-/-}$ mice were comparable, in terms of the number of TH-positive neurons in the SNpc, compared to wild-type littermates. However, *Parkin*$^{-/-}$ animals displayed a slight increase in striatal dopamine content, compared with wild-type littermates (not shown).

Parkin has been shown to ubiquinate Pael-R, thereby promoting degradation of insoluble and toxic Pael-R overexpressed in cell culture systems (6). Thus, we hypothesized that similar overexpression of Pael-R in *Parkin*$^{-/-}$ mice might result in severe ER stress and cell death in the SNpc. Using *Parkin*$^{+/+}$ and *Parkin*$^{-/-}$ mice, LoxPael-R was co-injected unilaterally into the striatum with LoxEGFP (as a neuronal marker) and S2NPNCre. Whereas up-regulation of Pael-R was confirmed by immunohistochemical analysis in the ipsilateral SNpc of both types of mice (white arrowheads in the lower panels of Fig. 3A indicate neurons positive with both TH and Pael-R), a marked decrease in the number of Nissl-positive neurons was demonstrated in *Parkin*$^{-/-}$ mice, (Fig. 3A and B). Neurodegeneration in the SNpc was accompanied by loss of TH immunointensity and decreased dopamine content in the striatum (Fig. 3C and D).

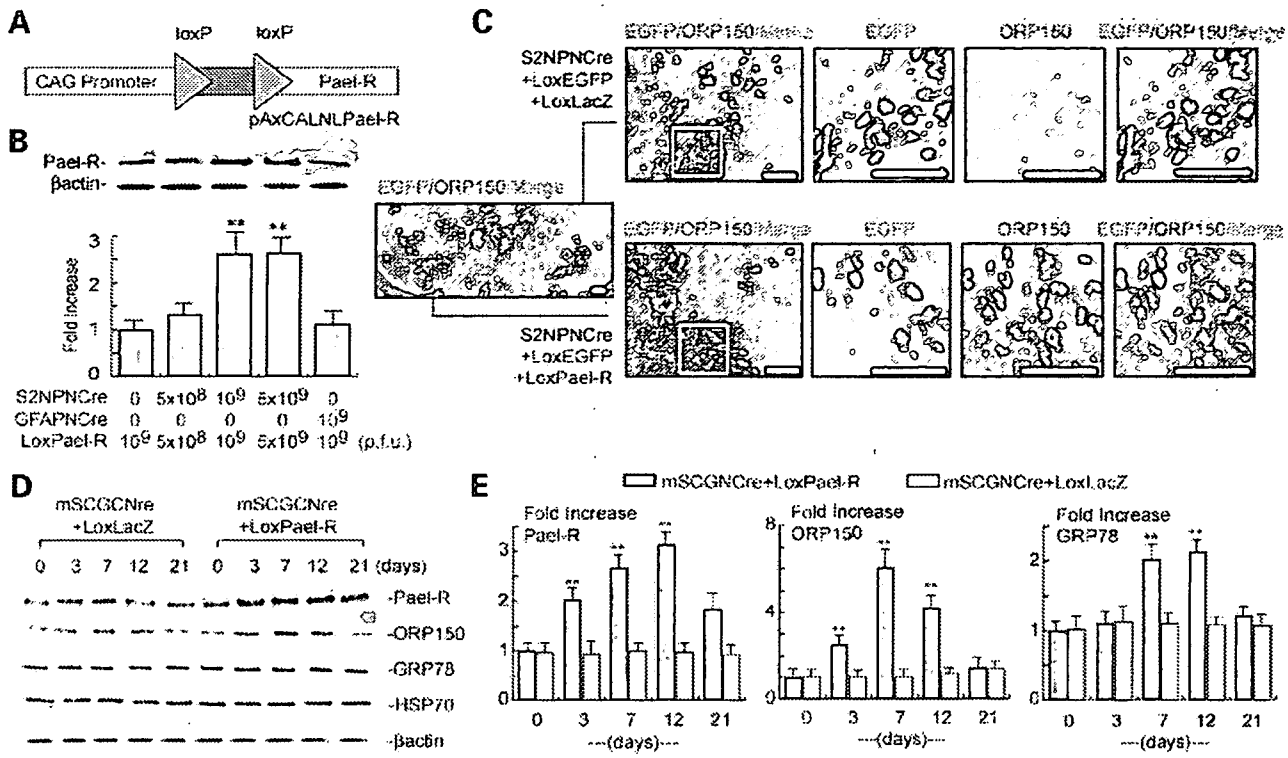

Figure 2. Transfection of Pael-R induces the ER stress in the SNpc. (**A**) Schematic depiction of the construct pAxCALNLPael-R to yield the adenoviral vector AxCALNLPael-R (LoxPael-R). A stuffer sequence (gray box) flanked by two lox-P sequences (arrowhead) was inserted between the promoter and *Pael-R* gene. (**B**) Adenoviral vectors carrying either S2NPNCre, GFAPCre or LoxPael-R were injected into the striatum as described in Figure 1, and, 7 days later, expression of Pael-R was assessed by Western blotting (upper panel), together with the levels of ß-actin as an internal control. Intensity of the corresponding bands was semi-quantitatively assessed by densitometric analysis and expressed in terms of fold-increase versus control samples where no adenovirus was injected (lower panel; $n = 6$, mean ± SD, and ** denotes $P < 0.05$ compared to LoxPael-R infection alone). (**C**) A mixture (total 2 μl) of adenoviral vectors including S2NPNCre (10^9 p.f.u.), LoxEGFP (5×10^8 p.f.u.), and AxCALNLNZ (LoxLacZ; 10^9 p.f.u.) was injected unilaterally in the striatum of C57Black/6J mice (upper panels). The same mixture was injected on the contralateral side, except that LoxLacZ was replaced by LoxPael-R (10^9 p.f.u.; lower panels). Seven days later, animals were perfusion-fixed and brainstem sections were immunostained using anti-ORP150 antibody (red). Merged images with EGFP signals (green) are shown in yellow. Open boxes indicated in the far left panels are magnified in the three panels on the right. Images are representative of six repeat experiments and the marker bar indicates 200 μm. (**D**) S2NPNCre + LoxLacZ (10^9 p.f.u., each) were injected unilaterally (termed ipsilateral) into the striatum, and S2NPNCre + LoxPael-R (10^9 p.f.u., each) were injected on the contralateral side. At the indicated time points, the brainstem was removed. The SNpc was separated and Western blotting was performed using antibodies to ORP150, GRP78, HSP70 and β-actin (images are representative of six repeat experiments). (**E**) Expression of Pael-R (left panel), ORP150 (middle panel), and GRP78 (right panel) on the ipsilateral (open bars) or contralateral side (closed bars) was assessed by densitometric analysis and is expressed as fold-increase versus control (day 0 indicates the day of the operation without injection of adenoviral vectors ($n = 6$, mean ± S.D is shown). ** denotes $P < 0.05$ by multiple comparison analysis compared to day 0 on the ipsilateral side.

No significant neuronal damage was observed in *Parkin*$^{+/+}$ mice after the overexpression of Pael-R using these methods.

To determine whether loss of TH staining in the SNpc, associated with increased expression of Pael-R, was due to neuronal death, we performed TUNEL analysis and monitored expression of a neo-epitope for activated caspase-3 (20). Increased expression of Pael-R in the SNpc, achieved as above (by unilateral injection of S2NPNCre, LoxPael-R and LoxEGFP; the contralateral side was injected with S2NPNCre, LoxLacZ and LoxEGFP as a control), demonstrated a small increase in DNA fragmentation even in the ipsilateral SNpc of wild-type mice (Fig. 4A and C). Increased DNA fragmentation was more striking in the ipsilateral SNpc of *Parkin*$^{-/-}$ mice, with maximal intensity 7 days after infection (Fig. 4B and C). The number of EGFP-and TUNEL-positive cells is significantly increased in the SNpc of *Parkin*$^{-/-}$ mice (Fig. 4B and C). It should be noted that there was a small increase in TUNEL staining on the contralateral side (Fig. 4C) observed most consistently in caudal sections (−3.4 and −3.6 from the Bregma). This might be due, at least in part, to crossed projections from the striatum to the contralateral SNpc. Pilot studies showed EGFP expression in the contralateral SNpc after unilateral injection of S2NPNCre and LoxEGFP, though this was <5% of the EGFP expression observed in the ipsilateral SNpc (not shown). Increased expression of Pael-R in the SNpc, achieved as above, demonstrated a small increase in the intensity of activated caspase-3 staining in the ipsilateral SNpc of wild-type mice (Fig. 4A and D). Expression of activated caspase-3 antigen was more striking in the ipsilateral SNpc of *Parkin*$^{-/-}$ mice (Fig. 4B and D), with maximal intensity 5 days after infection (not shown). The number of EGFP-positive cells costaining with activated caspase-3 is significantly increased in the SNpc of *Parkin*$^{-/-}$ mice (Fig. 4B and D).

Since there was no apparent damage, due to experimental manipulation or other factors, in the ipsilateral striatum (this

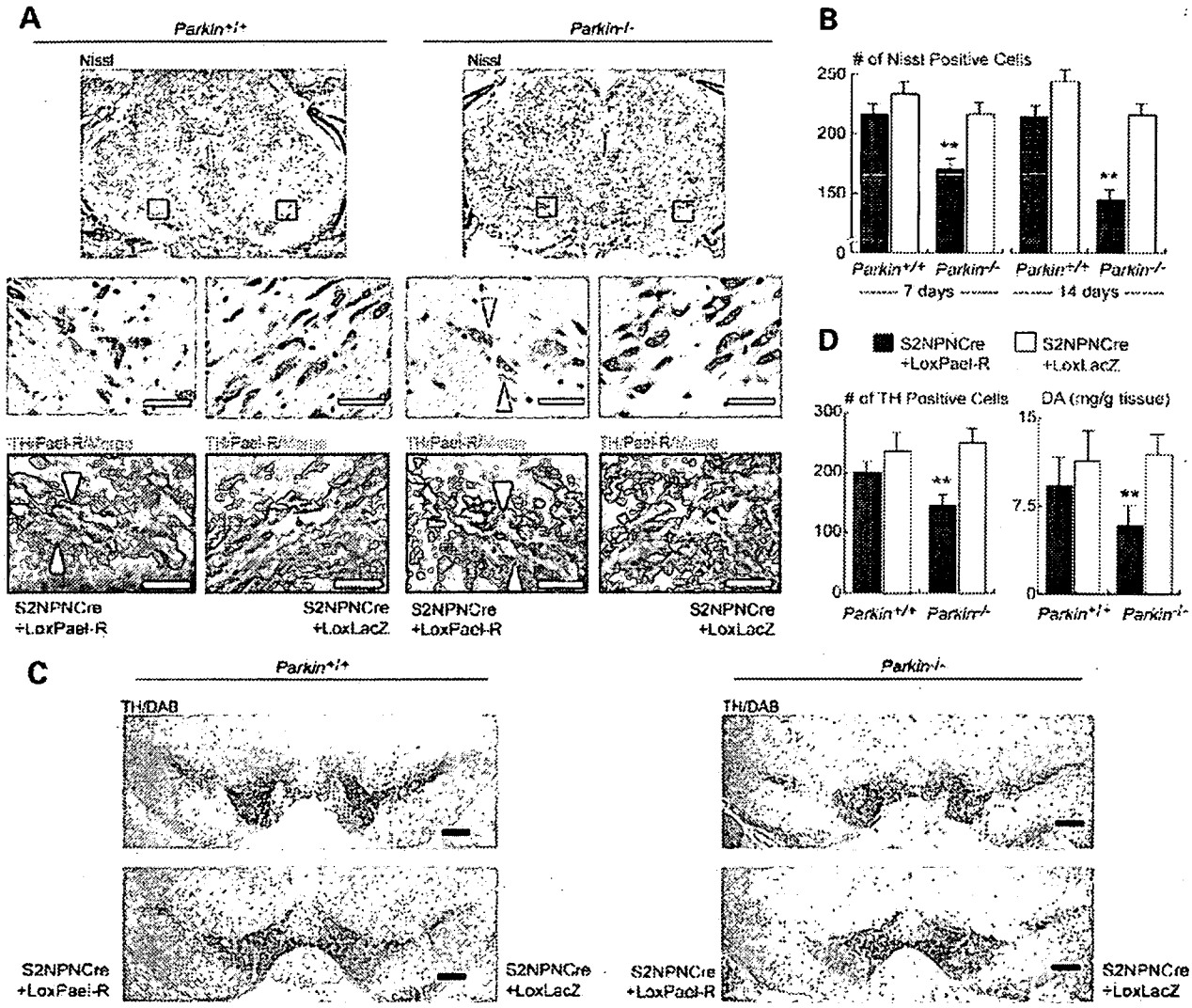

Figure 3. Enhanced neuronal death in the SNpc of parkin$^{-/-}$ mice by the up-regulation of Pael-R. (**A**) Adenoviral vectors (2 μl), including LoxEGFP (5×10^8 p.f.u.), S2NPNCre (10^9 p.f.u.) and LoxPael-R (10^9 p.f.u.) were injected unilaterally in the striatum of either parkin$^{+/+}$ or parkin$^{-/-}$ mice, as described in Figure 1. As a control, LoxPael-R was replaced by LoxLacZ (10^9 p.f.u.), and S2NPNCre + LoxLacZ was injected on the contralateral side. Brains of animals were then perfusion-fixed 7 days later, and midbrain sections were stained using the Nissl method (upper two panels). One of consecutive sections was also immunostained with anti-Pael-R antibody (lower panels). Images at −3.52 mM from the Bregma are shown. The open boxes in the upper panel are magnified in lower two panels. Typical examples of neurons positive with both TH and Pael-R are indicated by white arrowheads in the lower panels. Typical examples of degenerating neurons are identified by the open arrowheads in the middle panels. (**B**) Nissl positive neurons were counted on the ipsilateral (closed bars) and contralateral sides (open bars) as described in the text, 7 and 14 days after the injection. In each case, $n = 6$, and the mean ± SD is shown. ** denotes $P < 0.01$ compared to parkin$^{+/+}$ mice injected with LoxLacZ. (**C**) 10 days after the injection, midbrain sections were stained with anti-TH antibody as described in text. Images at −3.28 mM (upper panels) and −3.52 mM from the Bregma (lower panels) are shown. (**D**) TH positive neurons were counted 7 days after the injection (left panel). DA content was also measured by the HPLC-EC method 7 days after the injection (right panel). In each case, closed and open bars correspond to the ipsilateral (closed bars) or contralateral striatum (open bars) of parkin$^{-/-}$ or parkin$^{+/+}$ mice, respectively. In each case, $n = 6$, and the mean ± SD is shown. ** denotes $P < 0.01$ compared to parkin$^{+/+}$ mice injected with LoxLacZ.

side received injection of S2NPNCre, LoxPael-R and LoxEGFP) based on EGFP fluorescence or Nissl staining (Supplementary Material, Fig. S2B), diminished dopamine content most likely reflects loss of functional dopaminergic neurons in the ipsilateral SNpc. Moreover, injection of S2NPNCre and LoxPael-R resulted in the expression of Pael-R (marked by expression of EGFP) also in the motor cortex by retrograde infection (Supplementary Material, Fig. S2A). In contrast to the SNpc, no neuronal death was observed in either motor cortex or striatum (Supplementary Material, Fig. S2C). In other brain sublesions which have the connection to the striatum (i.e. the thalamus, the interpeduncular nucleus, the locus coeruleus and the raphe nucleus), no EGFP signals were detected, which may be due to the fewer communication to the striatum (not shown). The loss of TH immunointensity in the SNpc mainly occurred in neurons expressing Pael-R (Supplementary Material, Fig. S3A–C). These data suggest that Pael-R overexpression caused neuronal cell death, rather selectively in dopaminergic neurons in the SNpc.

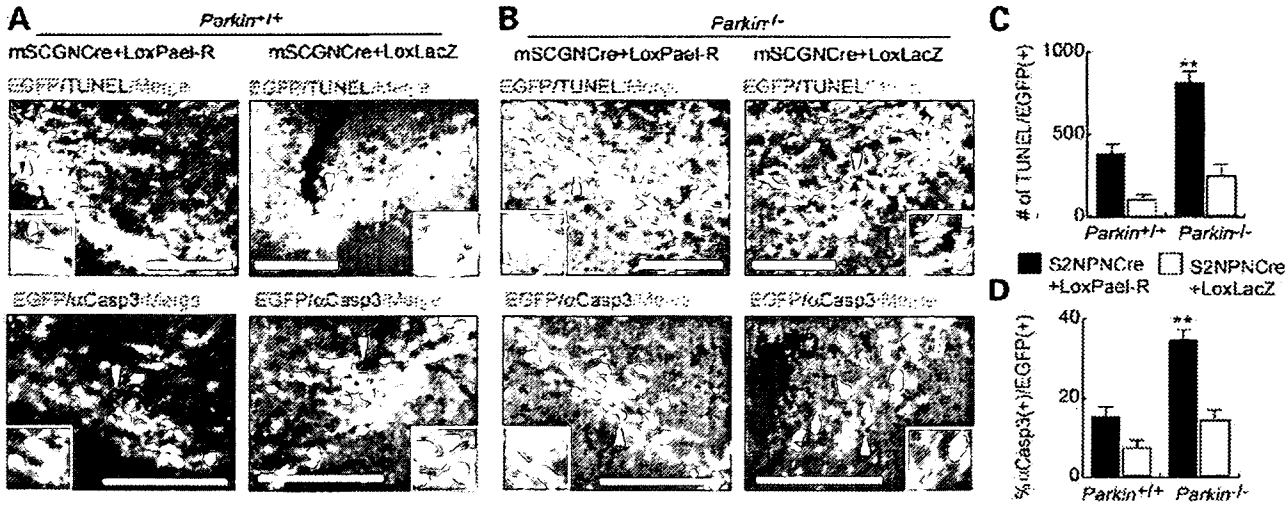

Figure 4. Assessment of neuronal cell death in parkin$^{-/-}$ mice (**A,B**) After infection of adenoviral vectors by the same protocol as used in Figure 3, brains of animals were perfusion-fixed 7 (upper panels for TUNEL) and 5 (lower panels for activated caspase-3 staining) days later, and midbrain sections were stained using either the TUNEL method or anti-activated caspase-3 antibody (αCasp3). Images at −3.52 mM from the Bregma were obtained to visualize the indicated antibody and the EGFP signal (green). In each panel, areas indicated by arrowheads are magnified in the insets at the lower corner of the panel. Note that TUNEL-positive and activated caspase-3-positive cells are increased in the EGFP positive area. Scale bar: 200 μm. Images shown in this figure (panels A,B) are representative of six repeated experiments. (**C,D**) Quantitation of TUNEL-positive signals (number of positive signals) 7 days after injection (panel C) or the percentage of cells positive for activated caspase-3 (αCasp3) in the population of EGFP-positive neurons 5 days after injection (panel D) on the ipsilateral (closed bars) or contralateral SNpc (open bars) of either parkin$^{-/-}$ or parkin$^{+/+}$ mice. In each case, $n = 6$, and the mean ± SD is shown. ** denotes $P < 0.01$ compared to parkin$^{+/+}$ mice injected with LoxLacZ.

ORP150 suppresses Pael-R-mediated neuronal cell death

These observations led us to hypothesize that ER stress might trigger loss of dopaminergic neurons due to accumulation of toxic Pael-R. To gain further insight into mechanisms underlying this observation, we focused on the function of an ER chaperone, ORP150, which promotes protein folding/degradation (17). We reasoned that if the ER stress is the cause of Pael-R-mediated dopaminergic neuron death, even in the presence of wild-type *Parkin*, decreased levels of ORP150 should accentuate Pael-R-induced neuronal death in the SNpc, whereas overexpression of ORP150 might be protective. Using targeted injection of adenoviral vectors (as above), Pael-R was overexpressed in the SNpc of either heterozygous *Orp150* truncation mutants [*Orp150*$^{+/-}$ mice; note, homozygous *Orp150*$^{-/-}$ mice have a developmental lethal phenotype 13)], strain-matched controls (*Orp150*$^{+/+}$ mice) or *Orp150* overexpressing wild-type transgenics [*Orp150* TG mice, driven by pCAGGS promoter (21)]. Elevated levels of ORP150 were confirmed in SNpc neurons of *Orp150* TG mice by immunohistochemical analysis (Supplementary Material, Fig. S4 upper panels; levels of ORP150 in strain-matched normal animals are also shown in lower panels). Degeneration of dopaminergic neurons was assessed by TUNEL staining and expression of activated caspase-3 (Fig. 5A and B), since these methods appeared to have adequate sensitivity, as shown in Figure 4. A gene dosage effect was observed; increased levels of ORP150 afforded protection to dopaminergic neurons. *Orp150*$^{+/-}$ mice, with the lowest levels of functional ORP150, displayed exaggerated damage to dopaminergic neurons; TUNEL staining and activated caspase-3 were enhanced on the ipsilateral SNpc (the side in which injection of adenoviral vectors resulted in over-expression of Pael-R; Fig. 5A and B), whereas no significant cell death was observed on the contralateral side where LoxLacZ was expressed (data not shown). Each of these indices of neuronal stress/toxicity in this setting was decreased, in a manner dependent on the 'dose' of *Orp150*, when the same experiment was performed in wild-type (*Orp150*$^{+/+}$) or mice overexpressing ORP150 (*Orp150* TG mice) (Fig. 5A and B).

These data suggest an essential contribution of ER function in protecting neurons from lethal toxicity when Pael-R is overexpressed. According to this concept, we further reasoned that such neurons in *Parkin*$^{-/-}$ mice might be rescued by either expression of Parkin or ER chaperones capable of promoting protein folding/renaturation, such as GRP78. Though adenoviral expression of LacZ in neurons failed to rescue SNpc neurons from Pael-R-mediated cell death, overexpression of Parkin minimized neuronal damage (Fig. 5C). Similarly, overexpression of GRP78 could substitute for Parkin in preventing Pael-R-mediated neuronal death in *Parkin*$^{-/-}$ mice. Western blot analysis of brain stem samples confirmed the expression of transfected gene products (Fig. 5C, right panel). These data indicate that the ER chaperones, such as GRP78 and ORP150, have the capacity to relieve ER stress due to increased expression of Pael-R, thereby exerting a protective effect on dopaminergic neurons in the SNpc.

Suppression of Pael-R-mediated cell death by inhibition of dopamine synthesis

Increased dopamine content in the striatum of *Parkin*$^{-/-}$ mice has been noted by some investigators, though the increase is small (18,19). Furthermore, Pael-R has been implicated in

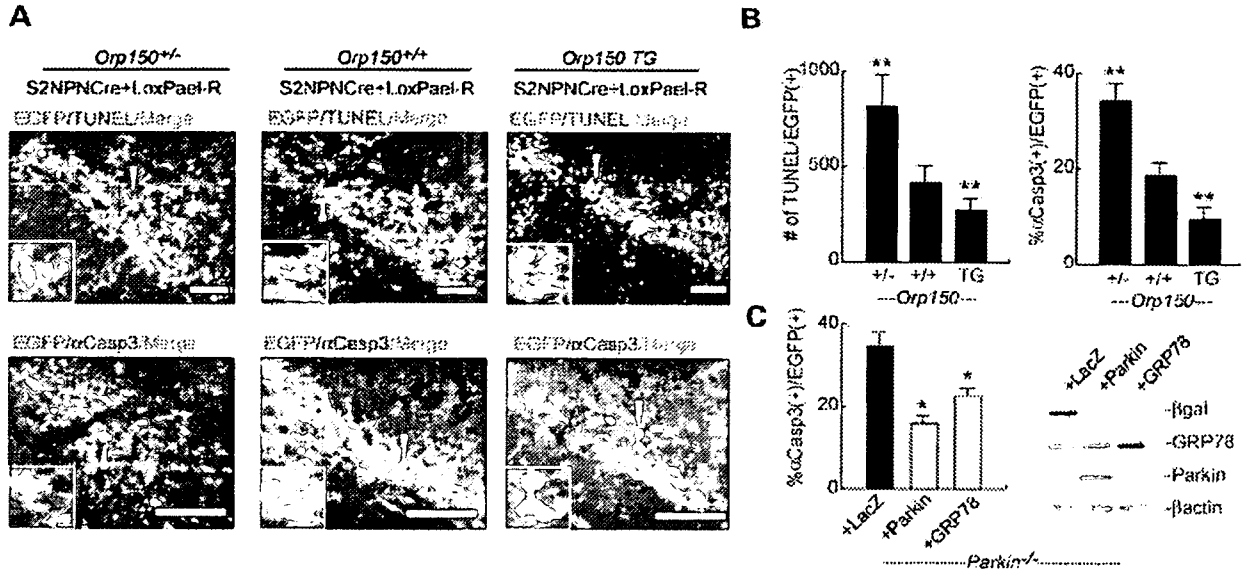

Figure 5. Effect of ORP150, Parkin, and GRP78 on Pael-R-mediated cell death in the SNpc. (**A**) Adenoviral vectors (2 μl), including LoxEGFP (5×10^8 p.f.u.), S2NPNCre (10^9 p.f.u.), and LoxPael-R (10^9 p.f.u.), were injected unilaterally into the striatum of either ORP150$^{+/-}$ (left panels), ORP150$^{+/+}$ (middle panels) or ORP150 transgenic mice (ORP150 TG; right panels) mice. Where indicated, LoxPael-R was replaced with LoxLacZ (10^9 p.f.u.), and the latter mixture was injected on the contralateral side. Brains were then perfusion fixed at 7 (for TUNEL analysis; upper panels) and 5 (for activated caspase-3 staining; αCasp3, lower panels) days after the injection. Images were overlapped with the EGFP signal (green). In each panel, the area indicated by the arrowhead is magnified in a small inset in the lower corner. Note the increase in cells staining positively by TUNEL analysis and for activated caspase-3 antigen in the EGFP positive area. This was most apparent in ORP150$^{+/-}$ mice. Scale bar: 200 μm. All images shown in this figure are representative of six repeated experiments. (**B**) Total number of TUNEL-positive signals (left panel) and the percentage of activated caspase-3 (αCasp3) positive cells in the population of EGFP-positive neurons (right panels) determined in the ipsilateral SNpc. In each case, $n = 6$, and the mean ± SD is shown. ** denotes $P < 0.01$ compared to ORP150$^{+/+}$ (wild type) mice. (**C**) A mixture (total 2 μl) of LoxEGFP (5×10^8 p.f.u.), S2NPNCre (10^9 p.f.u.), LoxPael-R (10^9 p.f.u.), and LoxLacZ (1.5×10^9 p.f.u.) was injected unilaterally into the striatum of parkin$^{-/-}$ mice. On the contralateral side, LoxLacZ was replaced with either AxCMParkin (Parkin; 1.5×10^9 p.f.u.) or AxCAGRP78 (GRP78; 1.5×10^9 p.f.u.). Midbrain sections were stained with anti-activated caspase-3 antibody (5 days later). The percentage of activated caspase-3-positive neurons was determined on the ipsilateral (closed bars) and contralateral sides. In the latter case, data is shown following injection of the vector expressing parkin (gray bars) and GRP78 (open bars) are shown. In each case, $n = 6$, and the mean ± S.D is shown. Midbrain samples collected from parkin$^{-/-}$ mice as described in text were also subjected to Western blot analysis using either anti-β-galactosidase, anti-GRP78, anti-Parkin or anti-β-actin antibody (for an internal control). A typical example of five repeated experiments is shown. * denotes $P < 0.01$ compared to the group injected with the vector expressing LacZ.

the regulation of dopamine levels; increased Pael-R is associated with increased dopamine content in the striatum (Imai, Y. *et al.*, manuscript in preparation). Based on these observations, we reasoned that Pael-R-mediated cell death in the SNpc of *Parkin*$^{-/-}$ mice might be associated with elevated levels of dopamine. Since dopamine has considerable potential toxicity (8,22), we further hypothesized that dopamine-derived metabolites/catabolites might contribute to loss of TH-positive (+) neurons. To address this issue directly, we determined whether suppression of DA synthesis by AMPT, a specific inhibitor of TH (15), would have a neuroprotective effect on TH(+) neurons overexpressing Pael-R in the SNpc of *Parkin*$^{-/-}$ mice. Accidental death of mice occurred in ≈4% of animals within 36 h after the first administration of AMPT. This might be due to the shifts of circadian temperature rhythms (23). The systemic toxicity of AMPT was not observed at later phase. Repeated administration of AMPT over a 7 day period lowered dopamine content of the striatum to ≈30% of that observed in untreated controls (Supplementary Material, Fig. S5). Using this protocol of AMPT treatment, adenoviral vectors were injected into the striatum to increase neuronal Pael-R levels in *Parkin*$^{-/-}$ mice. Compared with *Parkin*$^{-/-}$ mice treated with phosphate-buffered saline (PBS), animals receiving AMPT displayed striking neuroprotection. Inhibition of TH in *Parkin*$^{-/-}$ mice overexpressing Pael-R in the SNpc suppressed the number of TUNEL-positive nuclei and generation of activated caspase-3 epitopes, compared with animals treated with PBS alone (Fig. 6A–C). AMPT treatment was also effective in preventing Pael-R-mediated cell death in the SNpc of *Orp150*$^{+/-}$ mice, compared with animals treated with saline (Fig. 6C), suggesting a toxic effect of DA in ER dysfunction. These data suggest that dopamine enhances neurotoxicity associated with overexpression of Pael-R, especially in the absence of Parkin.

DISCUSSION

Our data indicate that *in vivo* overexpression of Pael-R in neurons of the SNpc results in enhanced ER stress, which, especially in a setting with decreased functional Parkin, targets TH-positive neurons for accentuated cytotoxicity. Whereas expression of a protein as difficult to properly fold as Pael-R has been shown to cause ER stress in a range of cell types *in vitro* (9), we believe that cellular vulnerability in this situation is critically exaggerated in dopaminergic neurons *in vivo* due to the superimposed toxicity of dopamine

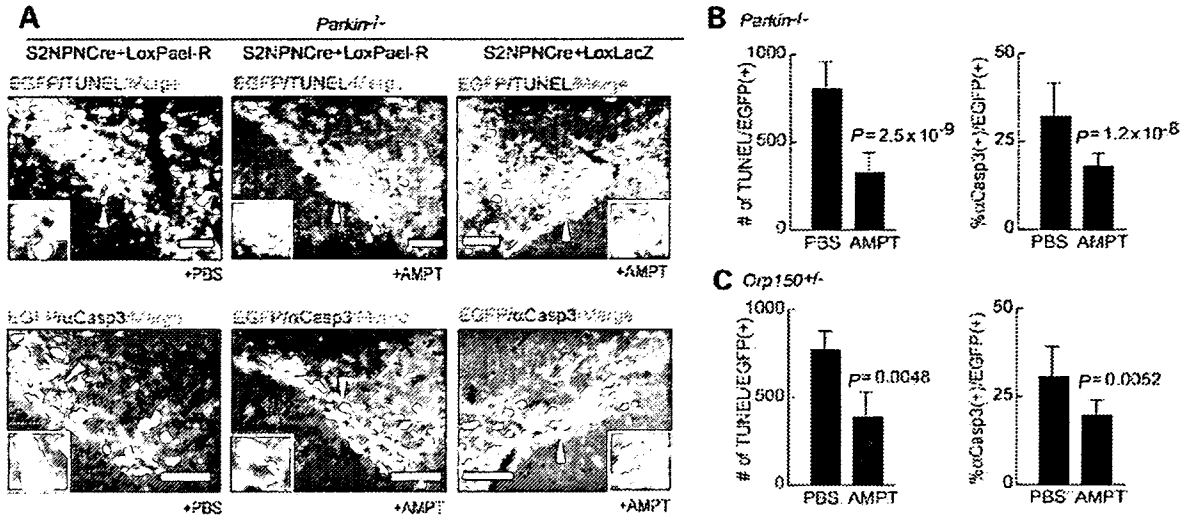

Figure 6. Suppression of neuronal death in the SNpc of mice overexpressing Pael-R by inhibition of dopamine synthetase using AMPT. (**A**) Parkin$^{-/-}$ mice were treated with either PBS or AMPT up to 7 days after unilateral injection of adenoviral vectors, including LoxEGFP (5×10^8 p.f.u.), S2NPNCre (10^9 p.f.u.) and LoxPael-R (10^9 p.f.u.). As a control, the same vectors, with LoxPael-R replaced by LoxLacZ (10^9 p.f.u.), were injected on the contralateral side. Brains were perfusion-fixed at 7 (upper panels; for TUNEL analysis) and 5 (lower panels; staining for activated caspase-3, αCasp3) days after injection of the vectors, and were then subjected to histochemical analysis as described above. The above images were overlapped with EGFP (green). Scale bar: 200 μm. All images shown in this figure are representative of six repetitions of the experimental protocol. In each panel, the area indicated by the arrowhead is magnified in a small inset in the lower corner. Note that TUNEL-positive and activated caspase-3-positive cells were diminished by AMPT treatment (i.e. in the presence of the latter, the area/level of apoptotic cells approximated that observed in controls overexpressing LacZ). (**B,C**) Statistical analysis was performed as described above, in either *Parkin*$^{-/-}$ mice (B) or *Orp150*$^{+/-}$ mice (C). The number of TUNEL-positive signals (left panels), and % of activated caspase-3-positive cells in the population of EGFP-positive neurons (right panels) in the ipsilateral SNpc are shown ($n = 6$; the mean ± SD). *P*-values,obtained by Student's t-analysis, are shown in each panel.

(DA) itself. These data also emphasize the potential relevance of parkin targets, such as Pael-R, in addition to the aminoacyl-tRNA synthetase cofactor p38, to neurotoxicity in dopaminergic neurons (24).

The technical approach employed in our experiments, injection of adenovirus under stereotactic guidance into the striatum with selective neuronal expression of gene products, is quite unique. First, such results have been difficult to achieve in the mouse because of anatomic limitations. Though adenovirus vectors are more immunogenic than adenovirus associated virus, they still have greater merits in retrograde transfection (25). We have taken this advantage into our experimental system, to achieve an efficient gene transfer to SNpc, where direct injection of viral vectors will be inapplicable because of anatomical limitations. Second, adenovirus infection predominately affects glia, rather than neurons. Modification of the SCG10 (superior cervical ganglion) promoter by tandem insertion of two neuron-restrictive silencers produced almost 100% expression of transgenes in neuronal cultures, and considerably lower expression in astrocytes (not shown). Coinjection of S2NPNCre with LoxEGFP into the striatum resulted in expression of transgenes in neurons of the mouse SNpc. This approach allowed us to obtain neuron-specific expression of Pael-R enabling study of its effect(s) on neuronal physiology *in vivo*. The proximal result of such Pael-R expression included upregulation of ER chaperones, such as GRP78 and ORP150, whereas the distal result was loss of TH-positive neurons, especially in *Parkin*$^{-/-}$ mice. In contrast, expression of Pael-R had no effect on the constitutively expressed form of HSP70, important for housekeeping functions in the cytoplasm (Fig. 2D).

Several observations are consistent with the importance of ER stress as a mechanism underlying Pael-R-induced cellular toxicity. In previous studies using cultured neuroblastoma cells, Pael-R has been identified as a substrate of Parkin, an E3 ubiquitin ligase (6). Thus, in the absence of Parkin, Pael-R may accumulate since it is not subject to efficient removal. In contrast, no detectable change of Pael-R levels has been reported in SNpc of Parkin null mice (24). Since there is no evidence of progressive neuronal cell death in Parkin null mice, there would appear to be redundant mechanisms able to compensate for loss of Parkin under physiologic conditions. The ability of neurons to withstand ER stress imposed by expression of Pael-R is likely to be dependent on the effectiveness of the ER-stress response; higher levels of Pael-R would require a facile ER-stress response (i.e. adequate or increased levels of parkin, ORP150, GRP78 etc), whereas diminished levels of ORP150 or GRP78 would render neurons vulnerable to toxicity because of a compromised stress response. These predictions have been borne out by our experimental results. Therefore, the possible toxicity of Pael-R cannot be completely ignored, especially in pathological conditions. Increasing expression of GRP78 had a protective effect in *Parkin*$^{-/-}$ mice overexpressing Pael-R. Furthermore, expression of ORP150, an important factor modulating ER stress even in the presence of Parkin, modulated the toxicity of Pael-R for dopaminergic neurons; increased levels of ORP150 in transgenic mice were neuroprotective, whereas diminished levels in ORP150 in *Orp150*$^{+/-}$ mice resulted in enhanced cell death (i.e. increased TUNEL staining and immunoreactivity for activated caspase-3 in the SNpc).

Our experimental system produced Pael-R overexpression and subsequent cell death in the SNpc of mouse, whereas no apparent cell death occurred either in the striatum or in the motor cortex (Supplementary Material, Fig. S2C). Furthermore, we observed a neuroprotective effect of a TH inhibitor in the SNpc of mouse, suggesting that DA also contributes to Pael-R-induced cell death of dopaminergic neurons. Consistent with these results in our mouse models, studies in transgenic flies overexpressing Pael-R in most of neuronal populations also showed selective loss of dopaminergic neurons, though the mechanism of cellular degeneration is not fully understood (10). One plausible explanation for focusing toxicity on dopaminergic neurons is the oxidative stress caused by the presence of DA and its derivatives (1). Another possibility that DA might compromise the survival of dopaminergic neurons is a chemical inactivation of cellular proteins by addition of DA to sulfhydryl group of proteins. Recently, it has been reported that dopamine covalently modifies Parkin, a protein rich in sulfhydryl group, in dopaminergic cells, leading to increased Parkin insolubility and inactivation of its E3 function (22). Vulnerability of Parkin to modification by DA further impairs degradation of Pael-R. Thus, even in sporadic PD, DA might interfere in the degradation of certain proteins, such as Pael-R, by the inactivation of Parkin. Collectively, these data propose a model in which a combination of ER stress and DA-related stress plays an important role in degeneration of dopaminergic neurons in sporadic PD as well as PD caused by *parkin* mutations.

MATERIALS AND METHODS

Targeted disruption of the mouse parkin gene

Parkin$^{-/-}$ mice were generated using standard gene targeting techniques (26). A targeting vector was constructed with a 15.7 kb genomic DNA fragment containing exon 3 of the parkin gene (Supplementary Material, Fig. S1). The region containing exon 3 was replaced with a Floxed pgk-neo cassette. A DT-ApA cassette was flanked at the 5′-end of the homologous arm for negative selection (27). The linearized targeting vector was transfected into E14 (129sv) ES cells. Positive clones were selected by Southern blotting, and then injected into C57Bl/6J (B6) blastocysts. Offspring harboring the targeted allele were generated by crossing chimeric mice with B6 mice. Results of such crosses were confirmed by Southern analysis.

Reverse transcription–polymerase chain reaction analysis of parkin null mice

Total RNA was extracted from whole brain tissue using Isogen (Nippon gene). RT reactions containing 1 μg of total RNA were performed using the SuperScript II First-Strand Synthesis System for RT–PCR (Invitrogen). The resulting cDNA was added to PCR reactions containing 1 unit of Ex *Taq* DNA Polymerase (Takara) for 35 PCR cycles. PCR products were separated on a 1% agarose gel. Primers were as follows: RT primer, 5′-agt ttc cct tga ggt tgt gc; Primer A, 5′-cgt agg tcc ttc tcg acc; Primer B, 5′-ttg agg ttg tgc gtc cag g; Primer C, 5′-acc tca gag ggc tcc ata tg; and, Primer D, 5′-ctc tct cta cac gtc aaa cca gtg.

Construction of adenoviral vectors

Modified SCG10 (S2NP10) promoter [2 kb (28)] and mouse GFAP promoter region (2.5 kb; kindly provided by Dr Ikenaka, National Institute for Physiological Science) were cloned into pAxAwNCre (kindly provided by Dr Saito, Tokyo University), a promoter-less cosmid vector for preparing cell type-specific Cre-recombinase expressing adenovirus (Fig. 2A; AxS2NPNCre and AxGFAPNCre). Human Pael-R (9) was cloned into pAxCALNLw (Takara Bio Inc., Shiga, Japan) in order to control Pael-R expression using Cre recombinase (AxLNLPael-R). The Pael-R gene is silenced because of the presence of the staffer of the neo-resistant gene, and is activated by Cre-mediated excisional deletion of the stuffer when a sufficient amount of Cre recombinase is expressed (Fig. 3). To prepare an adenoviral vector of parkin (AxCMParkin), the human parkin gene was cloned into pAxCMwt. Recombinant adenovirus was generating using the COS-terminal protein complex (TPC) method and the Takara adenovirus expression kit (Takara Bio Inc.). AxLNLNZ (Takara Bio Inc.), which overexpresses LacZ with a nuclear localization signal mediated by Cre recombinase, was used for control experiments. Cre-mediated EGFP-expressing adenovirus, AxLNLEGFP, was kindly provided by Dr Okado (Tokyo Metropolitan Institute of Neuroscience). An adenoviral vector for overexpression of GRP78/Bip (AxCAGRP78) was generously provided by Drs S. Tanaka and T. Koike [(29) Graduate School of Science, Hokkaido University]. Each adenovirus was amplified in HEK293 cells and purified using VIRAPREP Adenovirus Purification Kit (Virapur LLC., San Diego, CA, USA). Viral titers were determined by a plaque-forming assay in HEK293 cells.

Western blotting

Levels of Pael-R in tissue extracts were determined by Western blotting as described (9). Mouse brain was quickly removed and placed on a cold plate. Brain slices (200 μm) were obtained at −3.5 mM from the Bregma on a vibratome. Substantia nigra was then carefully removed under guidance of a stereoscopic microscope according to the mouse brain atlas (Paxinos and Franklin, Academic Press, 1997, San Diego) using the cerebral peduncle and medial lemniscus as landmarks. Tissue extracts were prepared from SNpc in PBS containing NP-40 (1%). Proteins were separated by SDS-PAGE, and transferred to PVDF. PVDF was then incubated with antibody to either human Pael-R or ß-actin, the latter as an internal control (1000 × dilution, Sigma, St Louis, MO, USA). Levels of chaperones in tissue extracts were determined by Western blotting, as described (30). PVDF was incubated with either anti-human ORP150 antibody (1 μg/ml), anti-GRP78 monoclonal antibody (Stressgen, Canada; 0.2 μg/ml), or anti-HSP73 antibody (0.1 μg/ml; Stressgen). Where indicated, either anti-β-galactosideas antibody (1000 × dilution, Sigma) or anti-Parkin antibody (1000 × dilution, Cell Signaling Technologies Inc.) was

used to access the level of these proteins. Images were further subjected to densitometric analysis using NIH image software.

Injection of adenoviral vectors into the striatum and treatment of animals

Animals were housed and treated according to institutional and national guidelines. Mice were stereotactically positioned under deep anesthesia, and the indicated combination of adenovirus vectors was injected unilaterally (a different combination, including a LacZ control, was injected on the contralateral side) into the striatum at six points (AP/ML/DV/ = 0.8/1.2/−2.5, 0.8/1.2/−3.2, 0.8/1.7/−2.5, 0.8/1.7/−3.2, 0.8/2.2/−2.5 and 0.8/2.2/−3.2; units are mm), followed by free access to food and water. Retrograde passage and infection of adenoviruses was confirmed 5–12 days after the injection by detection of a green fluorescent signal in the SNpc by fluorescence microscopy. Where indicated, animals were pretreated with α-methyl-DL-Tyrosine (AMPT) to suppress DA synthesis. AMPT-HCl (150 mg/kg, Sigma) was intra-peritoneally administrated twice per day for 5 days before injection of adenoviral vectors, as well as after the latter and until the day of sacrifice.

Assessment of neuronal death *in vivo*

At the indicated time points, animals were perfused with 4% paraformaldehyde under deep anesthesia, the brain was excised and coronal brain sections (14 μm) were cut on a cryostat. Sections were processed for cresyl violet staining or immunohistochemistry using either mouse anti-tyrosine hydroxylase antibody (TH; 1 μg/ml, Sigma), rabbit anti-human ORP 150 antibody [5 μg/ml (30)], rabbit anti-activated casepase-3 antibody(0.1 μg/ml, Genzyme/Teche), rabbit anti-Pael-R antibody [10 μg/ml, (9)] or goat anti-GFAP antibody (4 μg/ml. Santa Cruz Biotechnology, Santa Cruz, CA). Sections were also subjected to TUNEL staining using a commercially available kit (ApopTag, Intergen, Purchase, NY). To evaluate neuronal death in the SNpc, either Nissl or EGFP positive cells were counted in each coronal slice obtained at five different levels (−3.16, −3.28, −3.40, −3.52 and −3.64 mM from the Bregma), as described (31) by acquiring digital images using a CCD camera (Nikon, Coolscope). Cell death was semi-quantitatively assessed by counting TUNEL-positive cells/nuclei in the EGFP-positive area, and evaluating the percentage of activated caspase-3-positive cells in the population of EGFP-positive cells. Sections were analyzed using a laser scanning confocal microscope system (Leica, TCS SP2). In each case, two observers without knowledge of the experimental protocol evaluated sections and experiments were repeated at least three times.

DA content in the striatum was measured in the SNpc as described (32). In brief, striatal tissue was homogenized in solution H (0.4 M $HClO_4$ containing 4 mM $Na_2S_2O_5$, 4 mM diethylenetriaminepentaacetic acid, and 5 mM 1,4-dithiothreitol). Crude tissue lysate was separated on a C-18 reversed-phase column (MCM HPLC, 4.6 mM × 15 cm, 5 ml, ESA, Chelmsford, MA, USA), followed by electrochemical detection (Coulochem III, ESA).

Statistical analysis

Data shown represent the mean ± SD Multiple group comparisons were performed by one-way ANOVA, followed by Newman-Kuels test as a *post hoc* analysis. Comparison between two groups was analyzed by two-tailed Student's *t*-test.

SUPPLEMENTARY MATERIAL

Supplementary Material is available at HMG Online.

ACKNOWLEDGEMENTS

We thank Dr Martin Hooper (Western General Hospital, Edinburgh) for generous contribution of E14 cell line, and Drs Yumi Onodera, Yoshikazu Saito, Hitomi Suzuki (RIKEN, Wako, Japan) for technical assistance for establishing chimera mice. The authors also appreciate the generous gifts of AxCALNLEGFP, GAG promoter and Ax1CAGRP78 from Drs Haruo Okado (Tokyo Metropolitan Institute for Neuroscience), Jun-Ichi Miyazaki (Osaka University Medical School), and Shuuitsu Tanaka and Tetsuro Koike (Hokkaido University), respectively. This work was partially supported by the Ministry of Education, Science, Sports and Culture, a Grant-in-Aid for Scientific Research on Priority Areas—Advanced Brain Science Project—#15016120 to R.T., for Scientific Research (A) #14207032 to R.T., and for Young Scientists (A) #15680011 to Y.I. and a grant from the Special Postdoctoral Researcher Program of RIKEN to Y.I.

Conflict of Interest statement. None declared.

REFERENCES

1. Blum, D., Torch, S., Lambeng, N., Nissou, M., Benabid, A.L., Sadoul, R. and Verna, J.M. (1999) Molecular pathways involved in the neurotoxicity of 6-OHDA, dopamine and MPTP: contribution to the apoptotic theory in Parkinson's disease. *Trends. Biochem. Sci.*, **24**, 135–172.
2. Kitada, T., Asakawa, S., Hattori, N., Matsumine, H., Yamamura, Y., Minoshima, S., Yokochi, M., Mizuno, Y. and Shimizu, N. (1998) Mutations in the parkin gene cause autosomal recessive juvenile parkinsonism. *Nature*, **392**, 605–608.
3. Morett, E. and Bork, P. (1999) A novel transactivation domain in parkin. *Trends. Biochem. Sci.*, **24**, 229–231.
4. Jackson, P.K., Eldridge, A.G., Freed, E., Furstenthal, L., Hsu, J.Y., Kaiser, B.K. and Reimann, J.D. (2000) The lore of the RINGs: substrate recognition and catalysis by ubiquitin ligases. *Trends. Cell. Biol.*, **10**, 429–439.
5. Takahashi, R., Imai, Y., Hattori, N. and Mizuno, Y. (2003) Parkin and endoplasmic reticulum stress. *Ann. N.Y. Acad. Sci.*, **991**, 101–106.
6. Imai, Y., Soda, M. and Takahashi, R. (2000) Parkin suppresses unfolded protein stress-induced cell death through its E3 ubiquitin-protein ligase activity. *J. Biol. Chem.*, **275**, 35661–36664.
7. Shimura, H., Hattori, N., Kubo, S., Mizuno, Y., Asakawa, S., Minoshima, S., Shimizu, N., Iwai, K., Chiba, T., Tanaka, K. and Suzuki, T. (2000) Familial Parkinson disease gene product, parkin, is a ubiquitin-protein ligase. *Nat. Genet.*, **25**, 302–305.
8. Tanaka, K., Suzuki, T., Hattori, N. and Mizuno, Y. (2004) Ubiquitin, proteasome and parkin. *Biochim. Biophys. Acta.*, **29**, 235–247.
9. Imai, Y., Soda, M., Inoue, H., Hattori, N., Mizuno, Y. and Takahashi, R. (2001) An unfolded putative transmembrane polypeptide, which can lead to endoplasmic reticulum stress, is a substrate of Parkin. *Cell.*, **105**, 891–902.

10. Yang, Y., Nishimura, I., Imai, Y., Takahashi, R. and Lu, B. (2003) Parkin suppresses dopaminergic neuron-selective neurotoxicity induced by Pael-R in drosophila. *Neuron*, **27**, 911–924.
11. Tamatani, M., Matsuyama, T., Yamaguchi, A., Mitsuda, N., Tsukamoto, Y., Taniguchi, T., Che, Y.H., Ozawa, K., Hori, O., Nishimura, H. *et al.* (2001) ORP150 protects against hypoxia/ischemia-induced neuronal death. *Nat. Med.*, **7**, 317–323.
12. Miyazaki, M., Ozawa, K., Hori, O., Kitao, Y., Matsushita, K., Ogawa, S. and Matsuyama, T. (2002) Expression of ORP150 (150 kDa oxygen regulated protein) in the hippocampus suppresses delayed neuronal cell death. *J. Cereb. Blood Flow Metab.*, **22**, 979–987.
13. Kitao, Y., Ozawa, K., Miyazaki, M., Tamatani, M., Kobayashi, T., Yanagi, H., Okabe, M., Ikawa, M., Yamashima, T., Tohyama, M. *et al.* (2001) Expression of 150 kDa Oxygen Regulated Protein (ORP150), a molecular chaperone in the endoplasmic reticulum, rescues hippocampal neurons from glutamate toxicity. *J. Clin. Invest.*, **108**, 1439–1450.
14. Kitao, Y., Hashimoto, K., Matsuyama, T., Iso, H., Tamatani, T., Hori, O., Stern, D.M., Kano, M., Ozawa, K. and Ogawa, S. (2004) ORP150/HSP12A regulates Purkinje cell survival: a role for endoplasmic reticulum stress in cerebellar development. *J Neurosci.*, **24**, 1486–1496.
15. Dong, Z., Ferger, B., Paterna, J.C., Vogel, D., Furler, S., Osinde, M., Feldon, J. and Bueler, H. (2003) Dopamine-dependent neurodegeneration in rats induced by viral vector-mediated overexpression of the parkin target protein, CDCrel-1. *Proc. Natl Acad. Sci. U.S.A.*, **100**, 12438–12443.
16. Kanegae, Y., Lee, G., Sato, Y., Tanaka, M., Nakai, M., Sakaki, T., Sugano, S. and Saito, I. (1995) Efficient gene activation in mammalian cells by using recombinant adenovirus expressing site-specific Cre recombinase. *Nucleic Acids Res.*, **23**, 3816–3821.
17. Bando, Y., Ogawa, S., Yamaguchi, A., Kuwabara, K., Ozawa, K., Hori, O., Yanagi, H., Tamatani, M. and Tohyama, M. (2000) The 150 kDa Oxygen Regulated Protein (ORP150) functions as a novel molecular chaperone in the protein transport of the MDCK cells. *Am. J. Physiol. (Cell Physiol.)*, **278**, C1172–C1182.
18. Itier, J.M., Ibanez, P., Mena, M.A., Abbas, N., Cohen-Salmon, C., Bohme, G.A., Laville, M., Pratt, J., Corti, O., Pradier, L. *et al.* (2003) Parkin gene inactivation alters behaviour and dopamine neurotransmission in the mouse. *Hum. Mol. Genet*, **12**, 2277–2291.
19. Goldberg, M.S., Fleming, S.M., Palacino, J.J., Cepeda, C., Lam, H.A., Bhatnagar, A., Meloni, E.G., Wu, N., Ackerson, L.C., Klapstein, G.J. *et al.* (2003) Parkin-deficient mice exhibit nigrostriatal deficits but not loss of dopaminergic neurons. *J. Biol. Chem*, **278**, 43628–43635.
20. Selimi, F., Doughty, M., Delhaye-Bouchaud, N. and Mariani, J. (2000) Target-related and intrinsic neuronal death in lurcher mutant mice are both mediated by caspaea-3 actvation. *J. Neurosci.*, **20**, 992–1000.
21. Bando, Y., Tsukamoto, Y., Katayama, T., Ozawa, K., Kitao, Y., Hori, O., Stern, D.M., Yamauchi, A. and Ogawa, S. (2004) ORP150/HSP12A protects renal tubular epithelium from ischemia-induced cell death. *FASEB J.*, **18**, 1401–1403.
22. Lavoie, M.J., Ostaszewski, B.L., Weihofen, A., Schlossmacher, M.G. and Selkoe, D.J. (2005) Dopamine covalently modifies and functionally inactivates parkin. *Nat. Med.*, **11**, 1214–1221.
23. Cahill, A.L. and Ehret, C.F. (1982) Alpha-methyl-p-tyrosine shifts circadian temperature rhythms. *Am. J. Physiol.*, **243**, R218–R222.
24. Ko, H.S., vonCoelln, R., Sriram, S.R., Kim, S.W., Chung, K.K., Pletnikova, O., Troncoso, J., Johnson, B., Saffary, R., Goh, E.L. *et al.* (2005) Accumulation of the authentic parkin substrate aminoacyl-tRNA synthetase cofactor, p38/JTV-1, leads to catecholaminergic cell death. *J. Neurosci.*, **25**, 7968–7978.
25. Barkats, M., Bilang-Bleuel, A., Buc-Caron, M.H., Castel-Barthe, M.N., Corti, O., Finiels, F., Horellou, P., Revah, F., Sabate, O. and Mallet, J. (1998) Adenovirus in the brain: recent advances of gene therapy for neurodegenerative diseases. *Prog. Neurobiol.*, **55**, 333–341.
26. Gomi, H., Yokoyama, T., Fujimoto, K., Ikeda, T., Katoh, A., Itoh, T. and Itohara, S. (1995) Mice devoid of the glial fibrillary acidic protein develop normally and are susceptible to scrapie prions. *Neuron*, **14**, 29–41.
27. Yanagawa, Y., Kobayashi, T., Ohnishi, M., Kobayashi, T., Tamura, S., Tsuzuki, T., Sanbo, M., Yagi, T., Tashiro, F. and Miyazaki, J. (1999) Enrichment and efficient screening of ES cells containing a targeted mutation: the use of DT-A gene with the polyadenylation signal as a negative selection maker. *Transgenic Res.*, **8**, 215–221.
28. Namikawa, K., Murakami, K., Okamoto, T., Okado, H. and Kiyama, H. (2006) A newly modified SCG10 promoter and Cre/loxP-mediated gene amplification system achieve highly specific neuronal expression in animal brains. *Gene Ther.*, **13**, 1244–1250.
29. Satoh, T., Furuta, K., Tomokiyo, K., Nakatsuka, D., Tanikawa, M., Nakanishi, M., Miura, M., Tanaka, S., Koike, T., Hatanaka, H. *et al.* (2000) Facilitatory roles of novel compounds designed from cyclopentenone prostaglandins on neurite outgrowth-promoting activities of nerve growth factor. *J. Neurochem.*, **75**, 1092–1102.
30. Kuwabara, K., Matsumoto, M., Ikeda, J., Hori, O., Ogawa, S., Maeda, Y., Kitagawa, K., Imuta, N., Kinoshita, K., Stern, D. *et al.* (1996) Purufucation and characterization of a novel stress protein, the 150 kDa oxygen regulated protein (ORP150), from cultured rat astrocytes, and its expression in ischemic mouse brain. *J. Biol. Chem.*, **279**, 5025–5032.
31. Kuhn, K., Wellen, J., Link, N., Maskri, L., Lubbert, H. and Stichel, C.C. (2003) The mouse MPTP model: gene expression changes in dopaminergic neurons. *Eur. J. Neurosci.*, **17**, 1–12.
32. Itoh, S., Katsuura, G. and Takashima, A. (1988) Effect of vasoactive intestinal peptide on dopaminergic system in the rat brain. *Peptides*, **9**, 315–317.

Pigment Cell Res. 20; 222–224

LETTER TO THE EDITOR

High levels of melanin-related metabolites in plasma from pink-eyed dilution mice

Kazumasa Wakamatsu[1]*, Tomohisa Hirobe[2,3] and Shosuke Ito[1]

[1]Department of Chemistry, Fujita Health University School of Health Sciences, Toyoake, Aichi 470-1192, Japan
[2]Radiation Effect Mechanism Research Group, National Institute of Radiological Sciences, Inage-ku, Chiba 263-8555, Japan
[3]Graduate School of Science and Technology, Chiba University, Chiba 263-8522, Japan
*Address correspondence to Kazumasa Wakamatsu, e-mail: kwaka@fujita-hu.ac.jp

Key words: slaty/recessive yellow/pink-eyed dilution/p protein/Tyrosinase/Tyrp2

doi: 10.1111/j.1600-0749.2007.00370.x

Dear Sir,

In mice, >120 genes are involved in the development, proliferation and differentiation of epidermal melanocytes, and more than half of those genes have been cloned and their functions elucidated (Bennett and Lamoreux, 2003). Mutations in many of these genes affect the quantity or quality of melanin produced that is usually measured by chemical determination of melanin content in cells or in hair. Whether mutations in specific genes differentially affect plasma levels of such melanin-related metabolites is not known. In this report, we reveal that pink-eyed dilution mice but not mice with mutations in the melanocortin-1 receptor (Mc1r) or the enzyme dopachrome tautomerase (Dct), exhibit extremely high plasma levels of these melanin-related metabolites.

Mammalian melanocytes produce two chemically distinct types of melanin pigments, the black to brown eumelanins and the yellow to reddish pheomelanins (Ito, 2003). Both eumelanin and pheomelanin are derived from the common precursor dopaquinone that is formed following the oxidation of tyrosine by tyrosinase. Dopaquinone is a highly reactive intermediate, and in the absence of thiol compounds it undergoes an intramolecular cyclization to give dopachrome through a redox reaction. However, intervention of this process with thiols such as cysteine gives rise exclusively to thiol adducts of dopa, termed cysteinyldopas, among which 5-*S*-cysteinyldopa (5-*S*-CD) is the major isomer. Dopachrome is spontaneously rearranged to give mostly 5,6-dihydroxyindole (DHI) with a trace of 5,6-dihydroxyindole-2-carboxylic acid (DHICA). However, the rearrangement of dopachrome to form DHICA is greatly accelerated by Dct, also termed tyrosinase-related protein-2, Tyrp2. Further oxidation of those indoles leads to the production of eumelanin, while cysteinyldopa adducts are oxidized to give pheomelanin. In melanocytes (and in hepatocytes), DHICA is *O*-methylated to give 6-hydroxy-5-methoxyindole-2-carboxylic acid (6H5MI2C) as a major isomer (Wakamatsu *et al.*, 1990).

Dct is the product of the *slaty/Dct* locus and is a member of the tyrosinase-related protein family. The *slaty* mutation changes an arginine to glutamine in the first copper binding domain of Dct, which reduces Dct function *c.* 80% compared with wild-type Dct in eye extracts. Moreover, Dct-mutant, immortalized melanocytes were recently found to have Dct activity at levels about one-third that of non-agouti black melanocytes (Costin *et al.*, 2005). In slaty melanocytes in primary culture, it has also been reported that the expression of Tyrp2/Dct was greatly reduced compared with melanocytes wild-type at that locus (Hirobe *et al.*, 2006). The *extension/Mc1r* gene at the *E* locus encodes Mc1r that is localized on the plasma membrane of melanocytes (García-Borrón *et al.*, 2005). Pigmentation is switched from the production of eumelanin to pheomelanin in recessive yellow (*e/e*) mice, which are homozygous for a loss-of-function mutation at the *extension* (*E*) locus (Hirobe *et al.*, 2007). The mouse *pink-eyed dilution* (*p*) locus greatly reduces the production of eumelanin in melanocytes and in the retinal pigment epithelium (Hirobe *et al.*, 2003). The product of the *p* gene is an integral membrane protein that localizes in melanosomes. The p protein seems to be involved in regulating the maturation of melanosomes and in the stabilization or trafficking of melanosomal membrane proteins. It has been proposed that the p protein controls the processing and transport of tyrosinase (Toyofuku *et al.*, 2002). Another theory is that the p protein mediates melanosomal pH (Ancans *et al.*, 2001). In this study, plasma levels of 6H5MI2C and 5-*S*-CD were analysed in mice with *slaty*, *recessive yellow* or *pink-eyed dilution* mutations, to determine whether the levels of those intermediates reflect the effects of those genic substitutions and to compare them with levels of melanin contents in hair.

Figure 1A summarizes the changes during development (0.5–7.5 days) in plasma levels of 6H5MI2C in

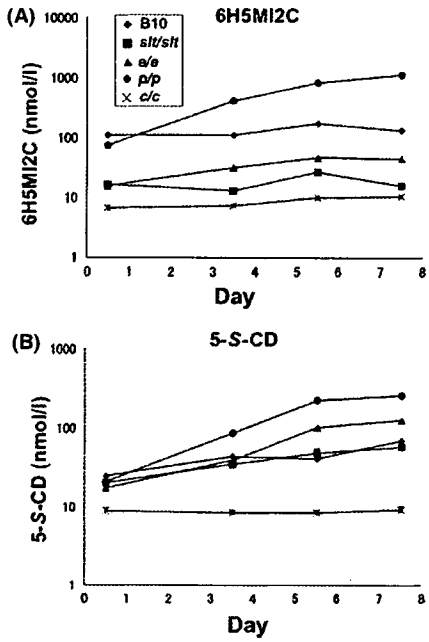

Figure 1 Changes in levels of (A) 6H5MI2C and (B) 5-*S*-CD in the plasma from 0.5-, 3.5-, 5.5- and 7.5-day-old C57BL/10JHir (black) mice and congenic *slt/slt* (slaty), *e/e* (recessive yellow), *p/p* (pink-eyed dilution), and *c/c* (albino) mice. Blood samples were collected from 0.5-, 3.5-, 5.5- and 7.5-day-old mice of all five strains from the carotid artery. Determination of 6H5MI2C in the plasma was performed using our previously reported method (Wakamatsu *et al.*, 1991) with minor modifications. Determination of 5-*S*-CD in the plasma was performed using HPLC with electrochemical detection, as previously reported by us (Wakamatsu and Ito, 1994) with a change of the plasma volume from 500 μl human serum to 10 μl mouse serum. Data are averages for three male and three female samples (one male and one female for *c/c* mice), each being taken from three to seven mice. There were no significant differences in plasma levels among male and female mice in each group, and thus the results present averages for all six samples. Standard errors of the mean (SEM) are smaller than symbols in most cases and are not shown.

C57BL/10JHir black mice (B10) and in congenic *slt/slt* (slaty), *e/e* (recessive yellow), *p/p* (pink-eyed dilution), and *c/c* (albino) mice. The black mice did not show any increase of 6H5MI2C during development with average levels of 144 nmol/l in their plasma. Similarly, levels of 6H5MI2C in plasma of *slt/slt* mice did not change significantly during the 7 day period, with an average level of 18 nmol/l which was sevenfold lower compared with black mice. Levels of 6H5MI2C in plasma of *e/e* mice showed a slight increase with age, from 16 nmol/l at 0.5 day to 45 nmol/l at 7.5 days. In contrast, levels of 6H5MI2C in plasma of *p/p* mice increased significantly with 74 and 1140 nmo/l at 0.5 and 7.5 days, respectively. The level of 6H5MI2C at 7.5 days in *p/p* mice was nine times greater than that in black mice. Albino mice gave a baseline level of 8.7 nmol/l on the average at all times examined. Figure 1B summarizes

Table 1. Plasma levels of 6H5MI2C and 5-*S*-CD in comparison with melanin contents in hair

	Plasma[a]		Hair[b]		
Phenotype	6H5MI2C (nmol/l)	5-*S*-CD (nmol/l)	PTCA[b] (ng/mg)	4-AHP[b] (ng/mg)	TM[b] (A_{500}/mg)
Black	134	70	1470	28	0.745
Slaty (*slt/slt*)	18	60	129	29	0.360
Recessive yellow (*e/e*)	70	127	9	2800	0.098
Pink-eyed dilution (*p/p*)	1140	258	70	91	0.051
Albino (*c/c*)	8.7	8.8	2	18	0.018

[a]Data are for 7.5-day-old mice.
[b]Most of the values are from unpublished studies, although similar data have been reported (Lamoreux *et al.*, 2001). Pyrrole-2,3,5-tricarboxylic acid (PTCA) is a specific degradation product from DHICA-derived eumelanin, while 4-amino-3-hydroxyphenylalanine (4-AHP) is from pheomelanin (Wakamatsu and Ito, 2003). Total melanin (TM) values were obtained by dissolving hair samples in Soluene-350 plus water (9:1, v/v) (Lamoreux *et al.*, 2001).

the changes during development (0.5–7.5 days) in plasma levels of 5-*S*-CD in C57BL/10JHir black mice (B10) and in congenic *slt/slt*, *e/e*, *p/p* and *c/c* mice. All four pigmented strains showed increased 5-*S*-CD levels with age. Black and *slt/slt* mice showed almost identical patterns of increases with 70 and 58 nmol/l at 7.5 days, respectively. Levels of 5-*S*-CD in *e/e* and in *p/p* mice at 7.5 days were 127 and 258 nmol/l, being 1.8 and 3.7 times higher than in black mice. Albino mice gave a baseline level of 8.8 nmol/l on the average at all time points.

Table 1 compares plasma levels of 6H5MI2C and 5-*S*-CD in 7.5 day newborn mice in comparison with melanin contents in hair. Mice mutant at the *slaty* locus (*slt/slt*) showed sevenfold lower levels of 6H5MI2C compared with black mice. This result is consistent with the greatly decreased activities of Dct in *slaty* mice (Costin *et al.*, 2005; Hirobe *et al.*, 2006) that lead to the production of DHI-rich and DHICA-poor eumelanin (Ito, 2003). The ratio of DHICA to DHI is known to correlate with the ratio of pyrrole-2,3,5-tricarboxylic acid (PTCA) to total melanin (TM) (Ozeki *et al.*, 1997). As shown in Table 1, *slaty* mice have a greatly reduced PTCA/TM ratio (360 ng/A_{500}) compared with black mice (1980 ng/A_{500}).

Recessive yellow (*e/e*) mice produce pheomelanic pigment in follicular melanocytes in vivo (Table 1). Those mice also show increases in the production of high levels of pheomelanin in the epidermis and dermis as the developmental age advances (Hirobe *et al.*, 2007). In the present study, plasma levels of 5-*S*-CD showed similar developmental increases. Moreover, the ratio of 5-*S*-CD/6H5MI2C levels in *e/e* mice was 2.8 at 7.5 days, while the ratio in black mice was 0.52, reflecting the type of pigmentation in those mice.

Pink-eyed dilution (*p/p*) mice produce greatly reduced (<1/10 that of black) levels of eumelanic pigment in follicular melanocytes in vivo (Table 1). However, in the present study, the plasma levels of 6H5MI2C and 5-*S*-CD in *p/p* mice at 7.5 days were ninefold and fourfold greater than in black mice. These results may appear surprising at first but are consistent with our finding that cultured *p/p* melanocytes fail to accumulate eumelanin and pheomelanin in the cells but release most of them (>90%) to the culture medium (Hirobe *et al.*, 2003). The dramatic increases in the plasma levels of 6H5MI2C and 5-*S*-CD after birth are also consistent with our previous results on the *p/p* melanocytes (Hirobe *et al.*, 2003).

The present study has demonstrated that the measurement of plasma levels of 6H5MI2C and 5-*S*-CD (in mice) provides useful information on the type of pigmentation. Of particular significance is the extremely high level of these melanin-related metabolites in pink-eyed dilution mice, suggesting the failure to accumulate melanin (and melanin-related metabolites) within melanocytes. The recent discovery of *SLC24A5*, a human orthologue of the zebrafish *golden* mutation, has stimulated renewed interests in the genetic basis of normal pigmentation variation seen within populations (Sturm, 2006). Several mutations in *SLC24A5*, *SLC45A2* (a human orthologue of mouse underwhite gene), and *OCA2* (a human orthologue of pink-eyed dilution gene) were found to be associated with light skin colours (Sturm, 2006). SLC24A5, SLC45A2 (also called MATP), and P protein are now thought to have similar roles in promoting melanin deposition through maturation of the melanosome. It would be thus interesting to compare the plasma levels of 6H5MI2C and 5-*S*-CD across various populations to see whether their release to the blood seen in mice is also a case in humans.

Acknowledgements

This work was in part supported by Grants-in-Aid for Scientific Research (no. 16591122) from the Ministry of Education, Science and Culture, Japan.

References

Ancans, A., Tobin, D.J., Hoogduijn, M.J., Smit, N.P., Wakamatsu, K., and Thody, A.J. (2001). Melanosomal pH controls rate of melanogenesis, eumelanin/pheomelanin ratio and melanosomal maturation in melanocytes and melanoma cells. Exp. Cell Res. *268*, 26–35.

Bennett, D.C., and Lamoreux, M.L. (2003). The color loci of mice – a genetic century. Pigment Cell Res. *16*, 333–344.

Costin, G.E., Valencia, J.C., Wakamatsu, K. *et al.* (2005). Mutations in dopachrome tautomerase (Dct) affect eumelanin/pheomelanin synthesis but do not affect intracellular trafficking of the mutant protein. Biochem. J. *391*, 249–259.

García-Borrón, J.C., Sánchez-Laorden, B.L., and Jiménez-Cervantes, C. (2005). Melanocortin-1 receptor structure and functional regulation. Pigment Cell Res. *18*, 393–410.

Hirobe, T., Wakamatsu, K., and Ito, S. (2003). Changes in the proliferation and differentiation of neonatal mouse pink-eyed dilution melanocytes in the presence of excess tyrosine. Pigment Cell Res. *16*, 619–628.

Hirobe, T., Wakamatsu, K., Ito, S., Kawa, Y., Soma, Y., and Mizoguchi, M. (2006). The slaty mutation affects eumelanin and pheomelanin synthesis in mouse melanocytes. Eur. J. Cell Biol. *85*, 537–549.

Hirobe, T., Wakamatsu, K., and Ito, S. (2007). The contents of eumelanin and pheomelanin present in female hairs of recessive yellow mice are greater in male hairs. J. Dermatol. Sci. *45*, 55–62.

Ito, S. (2003). A chemist's view of melanogenesis. Pigment Cell Res. *16*, 230–236.

Lamoreux, M.L., Wakamatsu, K., and Ito, S. (2001). Interaction of major coat color gene functions in mice as studied by chemical analysis of eumelanin and pheomelanin. Pigment Cell Res. *14*, 23–31.

Ozeki, H., Wakamatsu, K., Ito, S., and Ishiguro, I. (1997). Chemical characterization of eumelanins with special emphasis on 5,6-dihydroxyindole-2-carboxylic acid content and molecular size. Anal. Biochem. *248*, 149–157.

Sturm, R.A. (2006). A *golden* age of human pigmentation genetics. Trends Genet. *22*, 464–468.

Toyofuku, K., Valencia, J.C., Kushimoto, T., Costin, G.E., Virador, V.M., Viera, W.D., Ferrans, V.J., and Hearing, V.J. (2002). The etiology of oculocutaneous albinism (OCA) type II: the pink protein modulates the processing and transport of tyrosinase. Pigment Cell Res. *15*, 217–224.

Wakamatsu, K., and Ito, S. (1994). Improved HPLC determination of 5-*S*-cysteinyldopa in serum. Clin. Chem. *40*, 495–496.

Wakamatsu, K., and Ito, S. (2003). Quantitative analysis of eumelanin and pheomelanin in humans, mice, and other animals: a comparative review. Pigment Cell Res. *16*, 523–531.

Wakamatsu, K., Ito, S., and Fujita, K. (1990). Production, circulation, and excretion of melanin-related metabolites in B16 melanoma-bearing mice. Acta Derm. Venereol. *70*, 367–372.

Wakamatsu, K., Ito, S., and Horikoshi, T. (1991). Normal values of urinary excretion and serum concentration of 5-*S*-cysteinyldopa and 6-hydroxy-5-methoxyindole-2-carboxylic acid, biochemical markers of melanoma progression. Melanoma Res. *1*, 141–147.

Ann. Cancer Res. Therap. Vol. 15, No. 2, pp. 27-34, 2007

Heat immunotherapy with heat shock protein expression by hyperthermia using magnetite nanoparticles

Akira Ito[1], Takeshi Kobayashi[2], and Hiroyuki Honda[3]

[1] *Department of Chemical Engineering, Faculty of Engineering, Kyushu University,*
[2] *Department of Biological Chemistry, School of Bioscience and Biotechnology, Chubu University,*
[3] *Department of Biotechnology, School of Engineering, Nagoya University*

Abbreviations: heat shock protein, HSP; drug delivery system, DDS; magnetite cationic liposome, MCLs; antibody-conjugated magnetoliposome, AML; monoclonal antibody, MAb; natural killer, NK; metallothionein-I, MT; glucose-regulated protein 96, gp96; major histocompatibility complex, MHC; endoplasmic reticulum, ER; transporter associated with antigen processing, TAP; cytotoxic T lymphocyte, CTL; antigen-presenting cell, APC; dendritic cell, DC; nuclear factor, NF; tumor necrosis factor, TNF; interleukin, IL; macrophage inflammatory protein, MIP; macrophage chemotactic protein, MCP; regulated upon activation normal T cell expressed and secreted, RANTES; nitric oxide, NO; granulocyte macrophage-colony stimulating factor, GM-CSF; interferon, IFN.

Abstract

Hyperthermia is a possible approach for cancer therapy. However, a major technical problem associated with the use of hyperthermia is the difficulty of heating the local tumor region to the intended temperature without damaging normal tissue. Accordingly, in hyperthermia treatment, the expression of heat shock proteins (HSPs) has been considered a complicating factor because the expression of HSPs protects cells from apoptotic cell death. In cancer immunity, on the other hand, HSPs, including HSP70, have been shown to play an important role in immune reactions. If HSP expression induced by hyperthermia is involved in tumor immunity, novel cancer immunotherapy based on hyperthermia treatment can be developed. In such a strategy, a tumor-specific hyperthermia system that can induce necrotic cell death via HSP expression without damaging non-cancerous tissues would be highly advantageous. An intracellular hyperthermia system using functionalized magnetite nanoparticles, including magnetite cationic liposomes and antibody-conjugated magnetoliposomes, facilitates tumor-specific hyperthermia; this can induce necrotic cell death via HSP expression, which in turn induces antitumor immunity. We term this novel cancer therapy as "heat immunotherapy." This review discusses recent progress in cancer immunology via HSP expression and novel immunotherapy based on hyperthermia.

Keywords: Heat shock proteins, Hyperthermia, Tumor immunity, Magnetite

(Received July 9, 2007; Accepted August 10, 2007)

Introduction

Hyperthermia is a possible approach for cancer therapy. However, a major technical problem associated with the use of hyperthermia is the difficulty of heating the local tumor region to the intended temperature without damaging normal tissue. The rationale underlying hyperthermia is based on the fact that temperatures over 42.5°C are cytotoxic to tumor cells[1], particularly in an environment with a low pO_2 and low pH, conditions that are typically found in tumor tissue due to insufficient blood perfusion. At higher temperatures (e.g., 45–46°C), a greater number of tumor cells can be killed and, in principle, tumor-specific hyperthermia can kill all kinds of tumor cells because hyperthermia is a physical treatment and therefore would have fewer side effects than chemotherapy or radiotherapy.

Using magnetite nanoparticles, we have developed an intracellular hyperthermia system that can control local temperature within tumors. This novel hyperthermia treatment has produced unexpected biological responses, including overcoming thermotolerance due to specific heating of the tumor at high temperature, and an antitumor immune response induced by the expression of heat shock proteins (HSPs). These results suggest that our hyperthermia system can kill not only heated tumors but also non-heated tumors, including metastatic cancer cells. We have investigated the role of HSP70, which is a well-defined HSP, in order to elucidate the mechanism of immune induction by hyperthermia. In the present ar-

Correspondence to: Akira Ito, Ph.D., Associate Professor of Kyushu University, 744 Motooka, Nishi-ku, Fukuoka 819-0395, Japan. Tel: 81-92-802-2753, Fax: 81-92-802-2793, E-mail: akira@chem-eng.kyushu-u.ac.jp

ticle, the mechanism of the anticancer immune response induced by hyperthermia and new cancer immunotherapy based on the mechanism are reviewed and discussed.

Hyperthermia using magnetite nanoparticles

Various heating methods have been applied in hyperthermia[2]. However, an inevitable technical problem with hyperthermia is the difficulty of uniformly heating only the tumor region to the required temperature without damaging normal tissue. Accordingly, some researchers have proposed the use of "intracellular" hyperthermia to achieve a tumor-specific hyperthermia system, and have developed submicron magnetic particles (typically less than 100 nm in diameter) for this purpose.

In 1979, Gordon *et al.* first proposed the concept of intracellular hyperthermia. Magnetic iron oxide (Fe_3O_4, magnetite) particles of 6 nm diameter suspended in a sucrose solution were injected into a tail vain, and the selective uptake of particles by the tumor was observed by light and electron microscopy[3]. In 1999, Jordan *et al.* developed aminosilan-coated magnetite nanoparticles, in order to enhance the cellular uptake of the particles[4], and they demonstrated that intracellular hyperthermia exhibited greater cytotoxicity compared to water bath heating. When magnetite nanoparticles are used in *in vivo* study, the lack of colloid stability is an important issue. A possible approach to overcome these shortcomings of magnetic colloids is to coat magnetite nanoparticles with dextran; dextran magnetite was thus developed[5-7].

For drug delivery systems (DDS), liposomal coating is a promising approach. Shinkai *et al.* developed DDS techniques using liposomes for intracellular hyperthermia (Fig. 1A). The accumulation of magnetite nanoparticles in tumor cells can be enhanced by conferring a positive surface charge to the liposomal surface, and these authors have developed "magnetite cationic liposomes (MCLs)" with improved adsorption and accumulation properties[8]. MCLs, which have a positive surface charge, have 10-fold higher affinity for T-9 rat glioma cells than neutrally charged magnetoliposomes. Furthermore, a significant development in intracellular hyperthermia occurred when Shinkai and colleagues developed antibody-conjugated liposomes containing magnetite nanoparticles (antibody-conjugated magnetoliposomes, AMLs). They constructed immunoliposomes using mouse G22 monoclonal antibody (MAb) against human glioma cell lines[9], mouse G250 MAb against a human renal cell carcinoma cell line[10], and humanized MAb against human epidermal growth factor receptor-2 (Herceptin^R)[11], and demonstrated the tumor-specific targeting ability of these AMLs.

The first *in vivo* intracellular hyperthermia experiment was performed by Gordon *et al.* in 1979[3], using rats bearing mammary tumors. Non-coated magnetite nanoparticles were injected into a vein. Microscopic tissue analysis revealed that tumor cells had taken up particles. Two days after injection, the rats were exposed to a 450-kHz alternating magnetic field for 12 min. The tumor temperature increased by 8°C and histologic evidence of tumor necrosis was demonstrated. It was also reported that there were no side effects or toxicities associated with the use of the particles. Since the first *in vivo* experiment by Gordon, many researchers have reported encouraging results from intracellular hyperthermia using magnetite nanoparticles, including dextran magnetite[6,12] and aminosilane-coated magnetite[12,13]. One of the most systematic and comprehensive experiment using liposomal magnetite has been conducted by us (Fig. 1B). We have demonstrated the efficacy of intracellular hyperthermia using magnetite nanoparticles covered with liposomes in animals with several types of tumor, including B16 mouse melanoma[14], MM46 mouse mammary carcinoma[15], PC3 and LNCaP human prostate cancer in athymic mice[16], spontaneously developed primary melanoma in transgenic mice[17], T-9 rat glioma[18], Os515 hamster osteosarcoma[19], and VX-7 squamous cell carcinoma in rabbit tongue[20]. In these therapeutic experiments, MCLs were directly injected into solid tumors and the animals were irradiated several times (repeated hyperthermia) for 30 min with an alternating magnetic field of 118 kHz. The temperature of the tumor was elevated rapidly by magnetic heating and reached the intended temperature (42–46°C). In contrast, the rectal temperature or that in a tumor lacking the MCLs did not increase. After the alternating magnetic field irradiation, the tumor volume decreased markedly, and complete tumor regression was observed in 96% (46/48) of the animals in these experiments. These results indicate that MCLs are the superior tool for hyperthermia and that repeated hyperthermia using magnetite nanoparticles is a promising approach for cancer therapy.

We observed an antitumor immune response induced by hyperthermia using MCLs in an experimental T-9 rat glioma model in which a tumor was transplanted into each femur of a rat[21]. Interestingly, although only one tumor was subjected to hyperthermia, the other tumor also disappeared completely. Immunohistochemical assay revealed that natural killer (NK) cells and CD8- and CD4-positive T cells had migrated into the tumors after the hyperthermia treatment[21]. Here, T-9 rat glioma is a highly immunogenic cell line. Accordingly, our protocol was applied to a hereditary melanoma model; a primary skin melanoma developing in a metallothionein-I (MT)/*ret* transgenic mouse line[17]. In that study, in order to investigate whether an immune response could be induced after hyperthermia in MT/*ret* transgenic mice, the sizes of all the tumors that spontaneously occurred throughout the mouse body were measured. Each mouse (control group and hyperthermia group) had 8 tumors with sizes

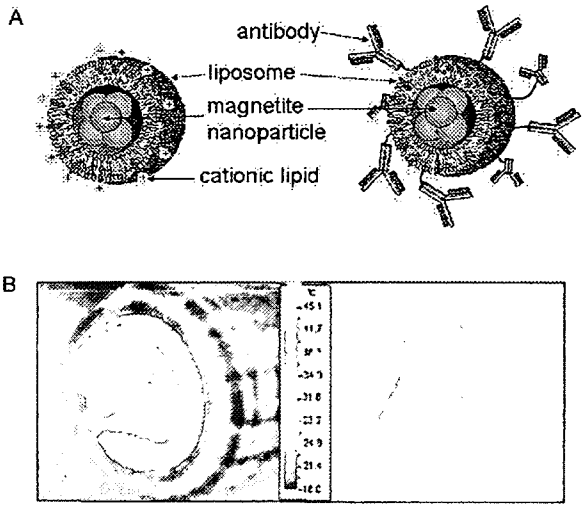

Fig. 1 Hyperthermia using magnetite nanoparticles.
(A) Liposomal drugs containing magnetite nanoparticles for drug delivery of magnetite nanoparticles. Left, magnetite cationic liposome (MCL); right, antibody-conjugated magnetoliposome (AML).
(B) Thermography of a mouse during hyperthermia using MCLs. MCLs were injected into the subcutaneous B16 tumors of mice and then an alternating magnetic field was irradiated. An alternating magnetic field was generated by a horizontal coil with a transistor inverter. The mouse was placed inside the coil. The left and right pictures are photographs of the mouse taken during and immediately after the alternating magnetic field irradiation, respectively. These pictures demonstrate that the MCL-mediated hyperthermia system is able to heat the tumor specifically.

ranging from 2 to 8 mm, which were located in the back and tail. In the control mice, all tumors grew and no tumor regression was observed. In the hyperthermia group on the other hand, although only 1 tumor was treated twice with hyperthermia, the other 3 tumors (2 on the back and 1 on the tail) also regressed and disappeared.

A mechanism of antitumor immunity induced by hyperthermia

HSPs were originally described with respect to their roles as chaperones induced by temperature shock as well as various other types of stress[22]. Recently, an additional role has been ascribed to HSPs as activators of the immune system. The importance of the HSP family, including HSP70, HSP90, and glucose-regulated protein 96 (gp96), in immune reactions has been demonstrated[23-26], and several researchers have reported that heat-treated tumor cells can play a vaccine-like role and elicit antitumor immunity[27-29]. With regard to the mechanism of antitumor immunity induced by hyperthermia using MCLs, our findings suggest 2 possible mechanisms of antigen presentation via HSP70 expression during hyperthermia[30-32]. One possible mechanism is the heat-induced augmentation of tumor immunogenicity due to the presentation of antigenic peptides via the major histocompatibility complex (MHC) class I antigens of tumor cells. Srivastava *et al.* proposed the "relay line model"[33-35] for tumor antigenic peptide transfer during antigen processing and presentation by HSPs (Fig. 2): The peptides digested by the proteasome are first bound to HSP70 or HSP90, which carry them to the endoplasmic reticulum (ER) via the transporter associated with antigen processing (TAP); the peptides are then transferred to gp96 in the lumen of the ER; and in the terminal step, gp96 transfers the peptides to the MHC class I $-\beta_2$ microglobulin complexes, and the tumor cell presenting the peptide via MHC class I is killed by MHC class I-restricted cytotoxic T lymphocytes (CTLs). Wells *et al.* demonstrated that stably transfected B16 melanoma cells that constitutively expressed human HSP70 exhibited significantly increased levels of MHC class I antigens on their surface[36,37]. We have demonstrated that augmentation of MHC class I antigens on the tumor cell surface via HSP70 expression causes immune induction[30]. In that study, HSP70 expression reached a maximum 24 h after heating, and the augmentation of MHC class I surface expression began 24 h after heating and reached a maximum 48 h after heating. In an *in vivo* experiment, the growth of T-9 cells in immunocompetent syngeneic rats was significantly inhibited by hyperthermia, with augmentation of MHC class I antigen surface

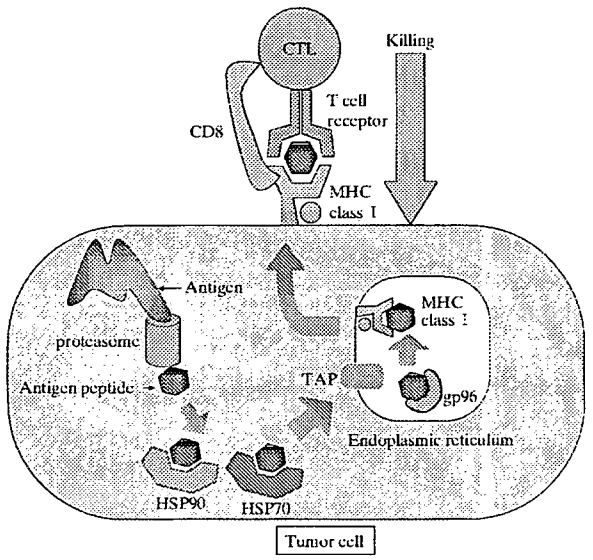

Fig. 2 Relay line model for tumor antigenic peptide transfer during antigen processing and presentation by heat shock proteins (HSPs). The HSP family, including HSP70 and HSP90 in the cytoplasm, and gp96 in the endoplasmic reticulum (ER), is involved in peptide transfer to MHC class I molecules. Details are described in the text.

expression. Conversely, the growth of T-9 cells in nude rats was not inhibited, suggesting that the effector cells were T lymphocytes. Furthermore, compared with lymphocytes from non-immunized rats or rats injected with non-heated T-9 cells, the splenic lymphocytes of rats injected with heated T-9 cells displayed specific cytotoxicity against T-9 cells. These results suggest that HSP70 is an important modulator of tumor cell immunogenicity during hyperthermia.

An alternative mechanism of recognition of tumor cell antigens by the host immune system in hyperthermia is the cross-presentation of antigenic peptides by dedicated antigen-presenting cells (APCs). HSP-mediated antitumor immunity may be caused by a vaccine-like effect of HSP-peptide complexes released from dying tumor cells. The released HSP-peptide complexes encounter APCs that express receptors such as CD91[38], CD40[39], and Toll-like receptors 2 and 4[40]. The interaction of HSP-peptide complexes with these receptors leads to receptor-mediated endocytosis, processing of the antigenic peptide by the endogenous MHC class I pathway, and re-presentation on the cell surface to CD8-positive T cell receptors[41]. Additionally, HSP70 functions as a direct activator of APCs, including dendritic cells (DCs)[42]. When HSPs bind to signaling receptors, such as CD14[42] and/or CD91 receptors[38], that trigger nuclear factor (NF)-$\kappa\beta$ activation[43], the DCs release pro-inflammatory cytokines including tumor necrosis factor (TNF)-α, interleukin (IL)-1β, IL-6, and IL-12[42, 44]; chemokines, including macrophage inflammatory protein (MIP)-1, macrophage chemotactic protein (MCP)-1, and regulated upon activation normal T cell expressed and secreted (RANTES)[45]; and nitric oxide (NO)[46], and up-regulate the expression of costimulatory and MHC class II molecules[43, 47, 48], resulting in the maturation of DCs[36]. This cytokine-like ability of HSP70 to stimulate the innate immune system is independent of the peptides they chaperone, suggesting that HSP70 is a natural adjuvant. Classical immunology theory is based on the distinction between "self and nonself"; however, this self-nonself model is sometimes not very useful, particularly in cancer immunity. Matzinger proposed the "Danger model," which suggests that the immune system is more concerned with damage than with foreignness[49, 50]. In the "Danger model," HSPs are considered an important "Danger signal." In particular, when HSPs, which are normally present in the cytoplasm, are released into the bloodstream, they can act as a signal to the immune system indicating an abnormal situation. We demonstrated that HSP70 expression following hyperthermia using MCLs induced antitumor immunity in rats with T-9 rat glioma[31]. Because MCLs are themselves heated in our hyperthermia system, the distribution of magnetite nanoparticles within tumors is an important issue. When MCLs were repeatedly heated, the surrounding tumor tissues underwent necrosis, and magnetite nanoparticles subsequently expanded into the necrotic area within the tumor, resulting in wide distribution of magnetite nanoparticles. Thus, the entire tumor area was necrosed by repeated (3 times) hyperthermia (with a 24-h interval over 3 days). The 24-h interval corresponded to the time when HSP70 expression in the T-9 cells reached its maximum, and a large amount of HSP70 was detected in the tumor tissue. Thus, our hyperthermia system using MCLs overcame thermotolerance and induced necrotic cell death that correlated with HSP70 expression. Next, we purified the HSP70-peptide complexes from the tumor after hyperthermia, and found that immunization of rats with T-9-derived HSP70 strongly suppressed tumor growth. HSP70-peptide complexes from liver (control) were also purified, and their vaccine effects were examined; however, no antitumor effects were observed. These results suggest that HSP70 in tumor cells chaperones some antigenic peptides after hyperthermia.

Although our hyperthermia system is designed to induce necrotic cell death, in order to induce HSP expression, there has been controversy in cancer immunology over whether vaccination with apoptotic cells or necrotic cells is more efficient. Apoptosis is programmed cell death, and is also considered "clean" cell death because the contents of the cells (including tumor antigens) are not released into the external environment but become packaged into the apoptotic body. In contrast, necrotic cell death is considered an unprogrammed event that is "not clean" because the cell contents are released into the environment. In necrotic cell death, as mentioned above, APCs including DCs can recognize antigens released from tumor cells via HSPs[43, 51]. In apoptosis, apoptotic bodies are engulfed by APCs, followed by antigen processing and presentation of tumor antigens by MHC class I antigens[52]. In fact, appropriate processing by APCs may occur in both apoptosis and necrosis. Apoptotic cell death would appear to be preferable to necrotic cell death because of the predictability of the results of apoptosis. When the complex program of apoptotic cell death is fully decoded, it will be possible to control the activation of a specific cascade of apoptotic events and induce apoptosis in any type of cancer using techniques such as molecular target therapy. However, at present, cancer therapy specifically designed to induce apoptosis do not appear to be feasible because cancer cells are adapted to escape from "death," particularly from apoptotic cell death, due to continual gene mutation. In contrast, it is relatively easy to induce necrotic cell death. Generally, when cells undergo extreme stress, they die in a necrotic manner. Yonezawa *et al.* examined the manner of cell death induced by hyperthermia[53]. Apoptotic cell death was induced in malignant fibrous histiocytoma cells by mild hyperthermia treatment at 42°C, whereas necrotic cell death was induced by hyperthermia at 44°C. Thus,

hyperthermia can easily induce necrotic cell death (in principle, in any type of tumor cell) by heating cells to a sufficiently high temperature. Our intracellular hyperthermia treatment can heat the tumor specifically via the MCLs. Moreover, the amount of heat generated in the tumor can be controlled by modulating the magnetic field intensity, making it possible to induce necrotic cell death without damage to the surrounding normal tissues. Another reason why necrotic cell death is effective for cancer therapy is that necrosis may strongly induce a "Danger signal." We observed that numerous and diverse kinds of immunocytes, such as CD8- and CD4-positive T-cells, NK cells, macrophages, and DCs, infiltrated into the necrotic area of tumors after hyperthermia treatment[21,31]. Todryk *et al.* observed infiltration of such cells into B16 melanoma nodules transfected with the HSP70 gene[54], suggesting that HSP70 expression is a "Danger signal" for the recruitment of immunocytes.

Taken together, the "passive release" of HSPs via heat-controlled necrosis by hyperthermia using MCLs is clearly an important methodology. Recently, on the other hand, an additional mechanism for HSP release has been proposed as "active release" [55]. Lancaster and Febbraio demonstrated that exosomes provide the major pathway for secretory vesicular release of the inducible type of HSP70[56]. In addition to containing HSP70, exosomes are densely packed with immunostimulatory mediators, including MHC class I and II[57] and costimulatory molecules[58]. Interestingly, psychological stress induced a marked increase in circulating HSP70; psychological stress induced by exposure of a rat to a cat resulted in the release of inducible type of HSP70[59]. Further studies remain to investigate whether hyperthermia treatment facilitates the active release of HSPs.

A proposed scenario in which HSPs function during successive stages of an antitumor response after hyperthermia is summarized and illustrated in Fig. 3.

Development of novel cancer immunotherapy based on heat-induced immune response via HSP expression

We are developing novel cancer immunotherapy based on the mechanism of anticancer immune response via HSP expression. Three key elements may be involved in the mechanism based on heat-induced immune response: (i) CTL as an effector cell, (ii) APC as an antigen-processing and antigen-presenting cell for HSP-peptide complex released from necrotic cells, and (iii) HSPs as natural and powerful immunostimulants.

Immunotherapy using cytokines has become an accepted therapeutic modality. We undertook these studies in order to study the combined effects of cytokines and hyperthermia using MCLs on melanoma[60]. MCLs were injected into a B16 melanoma nodule in mice, which were subjected to an alternating magnetic field for 30 min. The temperature at the tumor reached 43°C and was maintained by controlling the magnetic field intensity. At 24 h after hyperthermia, IL-2 or granulocyte macrophage-colony stimulating factor (GM-CSF) was injected directly into the melanoma. Mice were divided into 6 groups: group I (control), group II (hyperthermia), group III (IL-2), group IV (GM-CSF), group V (hyperthermia + IL-2), and group VI (hyperthermia + GM-CSF). Complete regression of tumors was observed in the mice of groups V and VI [75% (6/8) and 40% (4/10) of the mice, respectively], while no tumor regression was observed in mice of the other groups.

In addition, we conducted a screening of cytokines to enhance the vaccine effects of heated tumor cell lysate[61]. After heating mouse melanoma B16 cells (43°C, 30 min) to elicit increased HSP70 expression, the cells were lysed by freeze-thawing in order to prepare heat-treated cell vaccine. In approaches using poorly immunogenic melanoma B16, various cytokines (IL-1β, IL-2, IL-4, IL-6, and IL-12, interferon [IFN]-β and -γ, GM-CSF, and TNF-α) were assessed for combination with heat-treated cell vaccine. Syngeneic mice were immunized subcutaneously using heat-treated cell vaccine twice, on days –14 and –7, while cytokines were injected intraperitoneally on day –7. Subcutaneous B16 cell challenge was performed on day 0. IL-12 appeared to significantly enhance the vaccine effects of heat-treated cell vaccine, compared to non-heated cell lysate vaccine and non-vaccination. Systemic administration of recombinant IL-12 could augment the efficacy of heat-treated cell vaccine, inducing protective immunity against tumor challenge and enhance systemic cytotoxic activity in splenocytes against B16 cells in treated mice.

DCs are potent antigen-presenting cells that play a pivotal role in regulating immune responses in cancer and have recently been demonstrated to be activated by HSPs. For the use of APCs as antigen-processing and antigen-presenting cells for HSP-peptide complexes released from necrotic cells, DC therapy was combined with hyperthermia using MCLs[62,63]. In an *in vitro* study[62], when immature DCs were pulsed with mouse B16 cells heated at 43°C, MHC class I and II and costimulatory molecules CD80 and CD86 in the DCs were upregulated, thus resulting in DC maturation. Mice bearing a melanoma nodule were subjected to combination therapy using hyperthermia and DC immunotherapy *in vivo* by means of hyperthermia using MCLs and directly injected immature DCs. The mice were divided into 4 groups: group I (control), group II (hyperthermia), group III (DC therapy), and group IV (hyperthermia + DC therapy). Complete regression of tumors was observed in 60% of the mice in group IV, while no tumor regression was observed among the mice in the other groups. Increased CTL and natural killer (NK) activity was ob-